

1 Title: **Upper Plate Structure and Tsunamigenic Faults near the Kodiak Islands, Alaska**

2 Authors: Marlon D. Ramos<sup>1</sup>, Lee M. Liberty<sup>2</sup>, Peter J. Haeussler<sup>3</sup>, Robert Humphreys<sup>3</sup>

3 <sup>1</sup>*University of Michigan, Department of Earth and Environmental Sciences*

4 <sup>2</sup>*Boise State University, Department of Geosciences*

5 <sup>3</sup>*United States Geological Survey*

6

7 This work is a peer-reviewed preprint submitted to EarthArXiv. It has been recently accepted  
8 for publication at *Geosphere*, but has not undergone the official copyediting process.

9

10 *Social Media Twitter: @MarlonDRamos1*

11

12

13

14

15

16

17

18

19

20

21

22

23

24

25

26

27

28

29  
30  
31  
32  
33  
34  
35  
36  
37  
38  
39  
40  
41  
42  
43  
44  
45  
46  
47  
48  
49  
50  
51  
52  
53  
54  
55  
56  
57  
58  
59  
60  
61  
62

**Upper Plate Structure and Tsunamigenic Faults  
near the Kodiak Islands, Alaska**

Marlon D. Ramos<sup>1,2</sup>  
Lee M. Liberty<sup>2</sup>  
Peter J. Haeussler<sup>3</sup>  
Robert Humphreys<sup>3</sup>

<sup>1</sup>*University of Michigan, Department of Earth and Environmental Sciences*  
<sup>2</sup>*Boise State University, Department of Geosciences*  
<sup>3</sup>*U. S. Geological Survey*

Corresponding author:  
Marlon D. Ramos  
ramosmd@umich.edu  
<https://orcid.org/0000-0003-4449-8624>  
  
University of Michigan  
1100 North University Ave.  
Ann Arbor, MI 48109-1005

63 **ABSTRACT**

64 The Kodiak Islands lie near the southern terminus of the 1964 Great Alaska earthquake rupture  
65 area and within the Kodiak subduction zone segment. Both local and trans-Pacific tsunamis  
66 were generated during this devastating megathrust event, but the local tsunami source region  
67 and the causative faults are poorly understood. We provide an updated view of the tsunami  
68 and earthquake hazard for the Kodiak Islands region through tsunami modelling and  
69 geophysical data analysis. Using seismic and bathymetric data, we characterize a regionally  
70 extensive sea floor lineament related to the Kodiak shelf fault zone, with focused uplift along a  
71 50-km long portion of the newly named Ugak fault as the most likely source of the local Kodiak  
72 Islands tsunami in 1964. We present evidence of Holocene motion along the Albatross Banks  
73 fault zone, but suggest that this fault did not produce a tsunami in 1964. We relate major  
74 structural boundaries to active forearc splay faults, where tectonic uplift is collocated with  
75 gravity lineations. Differences in interseismic locking, seismicity-rates, and potential field  
76 signatures argue for different stress conditions at depth near presumed segment boundaries.  
77 We find that the Kodiak segment boundaries have a clear geophysical expression and are linked  
78 to upper plate structure and splay faulting. The tsunamigenic fault hazard is higher for the  
79 Kodiak shelf fault zone when compared to the nearby Albatross Banks fault zone, suggesting  
80 short wave travel paths and little tsunami warning time for nearby communities.

81

82 **INTRODUCTION**

83 Nearly the entire ~4000 km long Alaska-Aleutian subduction zone has ruptured in tsunamigenic  
84  $M > 8$  earthquakes during the last century (Plafker, 1969; Carver and Plafker, 2008; Ryan et al.,  
85 2011). Spatial and temporal distributions of these large earthquakes have given rise to the  
86 notion that the subduction zone is segmented (Nishenko and Jacob, 1990), with the  
87 presumption that different portions of the fault have unique earthquake cycles. The last  
88 rupture near the Kodiak Islands resulted from the  $M 9.2$  1964 Great Alaska Earthquake (GAE;  
89 Figure 1). This earthquake initiated from the slip patch, or asperity, affiliated with the Prince  
90 William Sound (PWS) segment, where uplift of up to 12 m was measured along the Patton Bay  
91 splay fault system (Plafker, 1969; Liberty et al., 2013). The slip extended through the Kenai  
92 segment (Suito and Freymueller, 2009), and terminated approximately 700 km to the  
93 southwest, beyond the Kodiak Islands (Johnson et al., 1996; Ichinose et al., 2007).

94

95 On the Kodiak Islands, local tsunami run-up was observed in 1964 (Kachadoorian and Plafker,  
96 1967; Figure 2), but sea floor displacements were not identified. The paleoseismic record shows  
97 evidence for many  $M 8+$  Holocene megathrust earthquakes associated with the Kodiak and

98 adjacent segments (Nishenko and Jacob, 1990; Hutchinson and Crowell, 2007; Carver and  
99 Plafker, 2008; Briggs et al., 2014; Shennan et al., 2014 and 2018), but the location, geometry  
100 and slip history of faults that splay from the megathrust is unknown. Given the robust  
101 paleoseismic evidence of large megathrust earthquakes, understanding this region's fault  
102 kinematics are important to seismic and tsunami hazard analysis and risk mitigation.

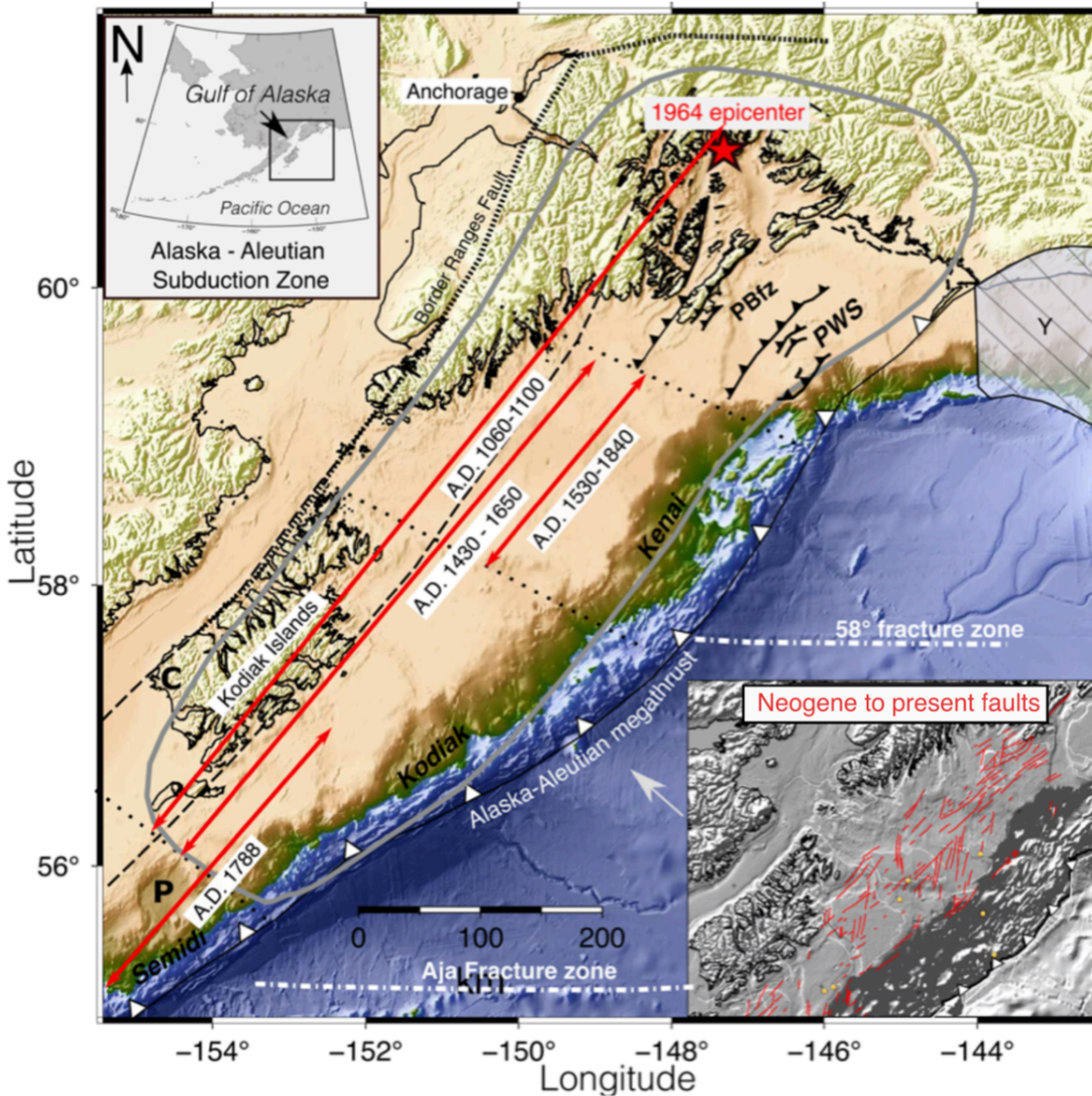
103

104 As most of the Gulf of Alaska forearc is submerged (Figure 1), paleoseismic studies have mostly  
105 relied on land elevation changes and the coastal sediment record to extract regional subsidence  
106 and uplift signals from earthquakes. However, these records do not uniquely constrain  
107 earthquake sources, cumulative slip estimates, or along-strike rupture limits from past  
108 earthquakes. Modern seismic, geodetic, and paleoseismic data suggest that M7+ earthquakes  
109 occur near the Kodiak Islands region every few decades, tsunami-capable M8 earthquakes have  
110 a median return-period of a hundred or more years, and multi-segment M9 great earthquakes  
111 have even longer return periods (Shennan et al., 2014). This temporal mismatch in coseismic  
112 behavior between the Kodiak segment and neighboring subduction zone segments suggest  
113 differences in strain accumulation and release along the plate interface which may be  
114 preserved in upper plate structures. The potential drivers of segmented megathrust ruptures  
115 and upper plate deformation may stem from the subduction of rough seafloor topography (e.g.,  
116 seamounts, fracture zones) or variable sediment volume and associated fluid content.  
117 Geophysical data have the potential to map active faults and to characterize along-strike  
118 variations in upper and lower plate structures that may uncover millennial-scale seismic  
119 behaviors.

120

121 In this paper, we identify and characterize faults in the region of the Kodiak segment using  
122 legacy and new bathymetric, seismic, and potential field datasets. We relate motion on these  
123 faults to both the GAE and other post Last Glacial Maxima (LGM) Holocene earthquakes. We  
124 use the distribution of mapped faults to characterize upper plate structure and to constrain the  
125 asperity boundaries and potential earthquake rupture limits. We use bathymetry data to back  
126 project first arrival tsunami travel times that were recorded during the 1964 earthquake and to  
127 identify tectonic scarps. We identify the faults that lie beneath these scarps with seismic  
128 reflection data and estimate splay fault geometries and uplift rates from these data. Finally, we  
129 use satellite free-air gravity and EMAG2 magnetic anomaly datasets (Maus et al., 2009;  
130 Sandwell et al., 2014) to infer upper plate deformation and assess signatures of segmentation  
131 around the Kodiak Islands.

132



133  
 134 **Figure 1.** Great Alaska earthquake (GAE) rupture area (gray line) with shaded relief topography  
 135 of the Gulf of Alaska region. Arrows denote rupture extent and age of previous megathrust  
 136 earthquakes (e.g., Carver and Plafker, 2008; Briggs et al. 2014; Shennan et al., 2014). Patton Bay  
 137 fault zone (PBfz) near Prince William Sound (Liberty et al., 2019) represents the region of  
 138 maximum uplift during the GAE. Dotted black lines denote inferred subduction zone segment  
 139 boundaries (Nishenko and Jacob, 1990; Suito and Freymueller, 2009). Inset map shows Neogene  
 140 and active seafloor scarps interpreted as mostly reactivated reverse or thrust faults (red lines).  
 141 Major fracture zone structures subducting below the Kodiak forearc include the Aja and 58°  
 142 fracture zones. Top inset represents the greater Alaska-Aleutian subduction zone. P=Prince  
 143 William Sound terrane, C=Chugach terrane, Y = Yakutat terrane. Colormap from Cramer (2018).  
 144

145

146 **TECTONIC SETTING**

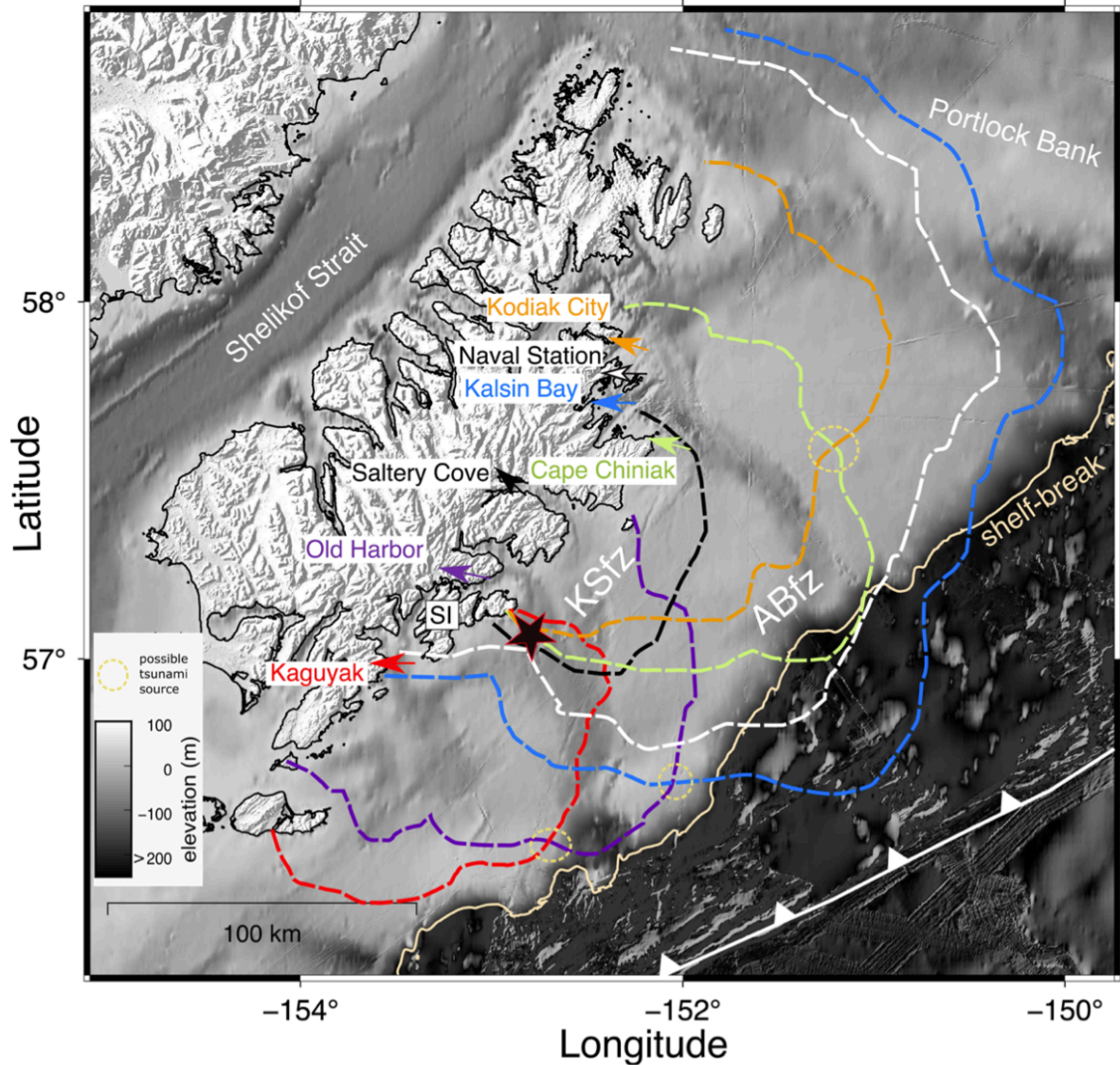
147 Tsunamigenic splay faults have been imaged within the Gulf of Alaska forearc with seismic and  
148 bathymetric data (von Huene et al., 2012; Liberty et al., 2013, Li et al., 2015, Haeussler et al.,  
149 2015, Liberty et al., 2019). Similar fault geometries and seafloor uplift patterns presumably  
150 span the length of this subduction zone, but differences in plate geometry and subducting  
151 structure may give rise to differences in forearc structures and earthquake potential. From  
152 teleseismic receiver function and crustal-scale active source seismic data across the Gulf of  
153 Alaska, we know that faults splay from the subduction interface where this megathrust dips to  
154 the north between three to nine degrees (Moore et al., 1991; Eberhardt-Phillips et al., 2006;  
155 Liberty et al., 2013; Kim et al., 2014; Haeussler et al., 2015; Becel et al., 2017, Hayes et al.,  
156 2018).

157

158 The Kodiak shelf fault zone (KSfz) and Albatross Banks fault zone (ABfz) have been inferred to  
159 control upper plate fault motions near the Kodiak Islands (Figure 2; Fisher and von Huene,  
160 1980; von Huene et al., 1980; Moore et al., 1991; Carver et al., 2008). Although no direct  
161 evidence has tied the KSfz and ABfz to the megathrust, we can presume that they splay from  
162 this boundary because of their similarity to splay fault structures already imaged on nearby  
163 subduction zone segments (e.g., Moore et al., 1991; Liberty et al., 2013; Haeussler et al., 2015;  
164 Becel et al., 2017).

165

166 Carver et al. (2008) mapped the on-land portion of the KSfz, and they named the largest fault  
167 the Narrow Cape fault. They determined a recurrence interval for surface displacing events on  
168 the fault of 1-2 ka, or more than five times longer than the average maximum recurrence  
169 interval for  $M > 8$  earthquakes on the Kodiak segment (e.g., Shennan et al., 2018). This suggests  
170 other faults may activate during large megathrust earthquakes. The trench-ward ABfz has been  
171 seismically imaged close to the continental shelf break and contains forearc basin-bounding  
172 reverse faults (Figure 2; Fisher, 1980; Fisher and von Huene, 1980). However, slip and fault  
173 distributions were poorly constrained due to a lack of modern seismic imagery; and there is no  
174 direct evidence that this fault system is active. In contrast, splay faults associated with the PWS  
175 and Semidi segments have been better characterized with more modern seismic and  
176 bathymetry surveys (e.g., Brocher et al., 1994; Liberty et al., 2013 and 2019; Finn et al., 2015;  
177 Haeussler et al., 2015; Li et al., 2015; Becel et al., 2017; Shillington et al., 2015). Here, we revisit  
178 legacy seismic data sets, and complement these older data with newly acquired seismic data to  
179 better constrain the tectonic history of the Kodiak segment.



180  
 181  
 182  
 183  
 184  
 185  
 186  
 187  
 188  
 189  
 190

**Figure 2.** Results from tsunami travel-time modelling along seven run-up locations across the Kodiak Islands. Back-propagated wave-fronts are colored according to run-up location and represent the maximum tsunami origin distance based on the first arriving wave crest. The star represents the estimated convergence region belonging to five tsunami wave-fronts and our preferred tsunami source that is ~15 km south of Sitkalidak Island. We term this tsunami-generating fault the Ugak fault. SI=Sitkinak Island. KSfz=Kodiak Shelf fault zone. ABfz=Albatross Banks fault zone.

191 **KODIAK SHELF BATHYMETRY**

192 For our tsunami source and fault mapping analysis, we utilize a regional bathymetry dataset to  
193 identify Kodiak shelf seafloor scarps (NOAA National Centers for Environmental Information,  
194 2004). The Southern Alaska Coastal Relief model for most of the continental shelf was compiled  
195 at a resolution of 24 arc-seconds, or a 720 m grid interval. We complement the regional  
196 bathymetry dataset with higher-resolution 8-arc second bathymetry data, and from a new  
197 compilation that covers the western Kodiak Islands region (Zimmerman et al., 2019). We  
198 recognize that much of the continental shelf region has not been surveyed within the past 50  
199 years, thus limiting our analyses. Regardless, our compilation shows that sea floor scarps  
200 related to the KSfz extend for at least 200 km, from offshore Sitkinak Island northeast to at least  
201 the Chiniak trough (Figure 3). These scarps are upwards of 50 m tall, greatest in height near  
202 Sitkalidak Island.

203

204 Most of Alaska's continental shelf has water depths of 100 m or less, and has been shaped by  
205 LGM ice loads, post-glacial deposition, and Holocene tectonism. Sea levels were approximately  
206 120 m below modern levels during the LGM (e.g., Peltier and Fairbanks, 2006) and ice covered  
207 much of the continental shelf (Kaufman and Manley, 2004; Kaufman et al., 2011). Radiocarbon  
208 dating at Narrow Cape indicates it was deglaciated approximately 13 – 13.5 kya (Figure 2, 3b;  
209 Carver et al., 2008), likely resetting seafloor surface prior to that time.

210

211 The shallow shelf areas typically contain little unconsolidated sediment that reflect modern  
212 deposition. In contrast, cross-shelf glacial troughs are often more than 50 m deeper than the  
213 nominal shelf depth and are traps for modern deposition (e.g., Carlson and Molnia, 1975;  
214 Liberty et al., 2013; 2019). These unconsolidated sediments typically lie above a prominent  
215 shallow unconformity that likely represents the hiatus in deposition during glaciation (e.g.,  
216 Figure 4e). Because many sea floor lineaments cross pre-Pleistocene depositional fabric, we  
217 assume that these represent scarps from Holocene fault uplift (e.g., Liberty et al., 2013; 2019).

218

219 **FIRST-ARRIVAL 1964 TSUNAMI SOURCE**

220 The 1964 GAE generated tsunamis that inundated shorelines around the Pacific Ocean. Plafker  
221 (1969) inferred a tsunami source from the continuation of the Patton Bay fault to have caused  
222 the first waves that arrived on the Kodiak Islands (Figure 2 and Table 1). However, the offshore  
223 extension of the Patton Bay fault was not mapped at that time. Subsequently, Liberty et al.,  
224 (2019) showed that Holocene activity along the Patton Bay fault system diminishes to the  
225 southwest of PWS as large scarps do not extend across the Kenai segment (Liberty, 2015; Figure



226 1). Suleimani and Freymueller (2020) evaluated the role of splay faults and horizontal  
227 displacements from several regional coseismic slip models from the GAE and found they both  
228 locally had significant contributions.

229

230 To identify coseismic uplift near the Kodiak Islands, we use modern bathymetry (Figure 3),  
231 seismic reflection data (Figure 4), and a compilation of GAE tsunami first arrival times (Table 1).  
232 We use tsunami first motions (estimated to the nearest minute) observed at seven sites on the  
233 Kodiak Islands relative to the main shock origin time (Plafker, 1969). We treat each run-up  
234 location as a wave source and back-propagate this source using finite differences (Figure 2). To  
235 derive a velocity field, we grid multi-beam and single beam bathymetry data at one-kilometer  
236 spacing and then convert depth to tsunami wave speed in each cell. We use La Grange's  
237 velocity-depth relationship,  $v = \sqrt{gd}$ , where  $d$  is the depth in meters and  $g$  is gravitational  
238 acceleration (Lamb, 1932). Each source is then back-propagated using this velocity field  
239 according to its respective tabulated travel time. We then compile individual wave-fronts from  
240 the final model to identify which sources could have shared the same tsunamigenic source  
241 location. Note that our approach cannot constrain tsunami wave amplitude and does not  
242 consider later arrivals; thus, we do not model near-shore, non-linear effects on tsunami wave  
243 propagation or identify additional tsunamigenic sources associated with later tsunami arrivals.  
244 Finally, we compare convergent source locations to identified trench-parallel scarps observed  
245 with seafloor topographic data and faults identified with seismic profiling.

246

247 The reported first sense of motion for some run-up locations was up, consistent with the Kodiak  
248 Islands being located landward of the hanging wall of the Alaska-Aleutian megathrust (Plafker,  
249 1969; Table 1). The one exception was at the northernmost Kodiak City measurement site. Of  
250 the seven tsunami sites, five back-projected wave-fields (Kaguyak, Saltery Cove, Cape Chiniak,  
251 Kalsin Bay, and Kodiak City) converge about 15 km south of Sitkalidak Island (Figure 2). Here, we  
252 find a conspicuous 50-m-high trench-parallel seafloor scarp that we associate with the KSfz  
253 (Figure 3). Two observations, Kalsin Bay and Old Harbor sites, do not share overlapping wave-  
254 fronts, and arrive too late to be sourced from this region. We note the reported first arrival  
255 time for Old Harbor is inconsistent with this interpretation; it is situated in a sheltered bay  
256 (Figure 2), and a direct tsunami wave from a fault located south of Sitkalidak Island may have  
257 experienced a more complex travel path. Thus, all but the measurement from Kalsin Bay is  
258 consistent with motion along the fault scarp near Sitkalidak Island (Figures 2 and 3).

259

260 We infer only part of the KSfz moved in the 1964 earthquake. Had the faults near Kodiak City  
261 experienced significant uplift, tsunami wave crests would have arrived sooner to the north  
262 (Figure 2). Similarly, onshore KSfz fault segments did not show evidence for uplift in 1964  
263 (Plafker, 1969; Carver et al., 2008). Thus, measurable uplift related to the GAE was likely limited  
264 to a narrow portion of the KSfz near the center of the Kodiak subduction zone segment.

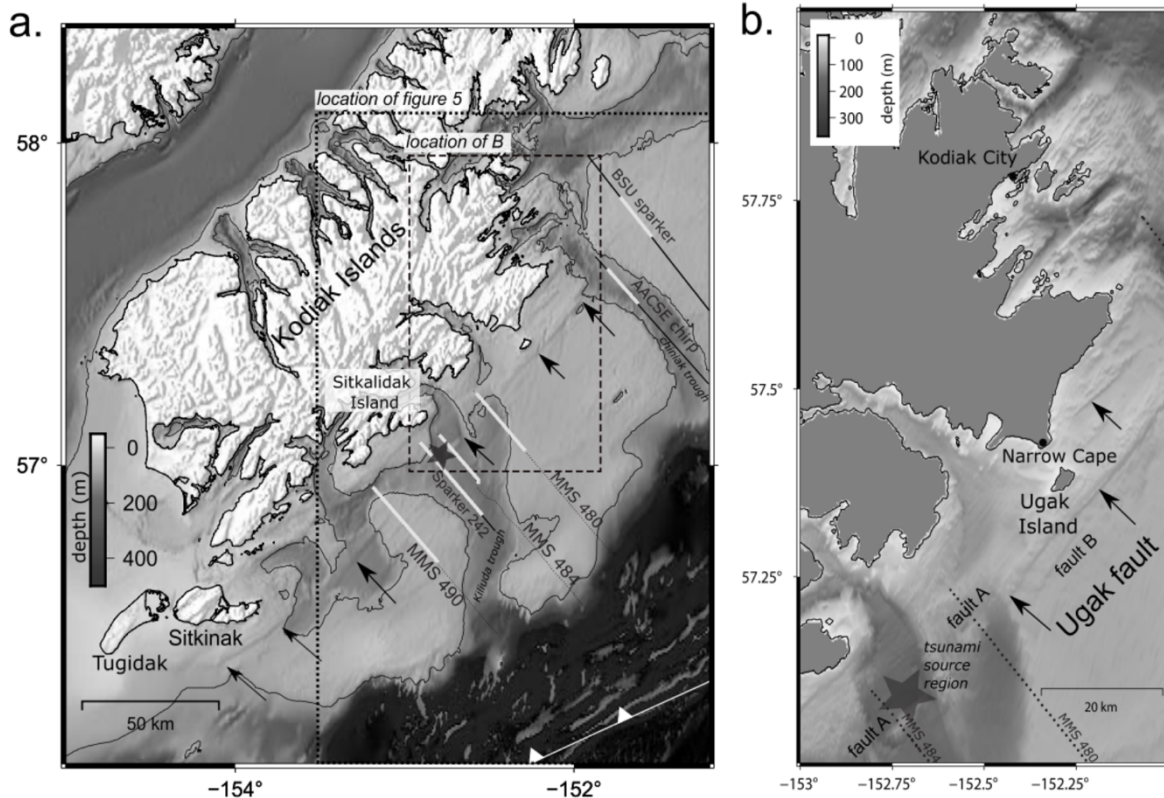
265  
266 We infer uplift along a short segment of the KSfz during the GAE, where KSfz seafloor  
267 lineaments have similar scarp heights along-strike (Figure 3). With scarp heights upwards of 50  
268 m, and an estimated maximum coseismic uplift per event of about 8 m (Plafker, 1969), we  
269 conclude that 1) the region surrounding GAE uplift has repeatedly ruptured during Holocene  
270 megathrust earthquakes, 2) additional along-strike faults associated with the KSfz have  
271 ruptured in a similar fashion during past megathrust earthquakes, and 3) the entire length of  
272 this fault should be considered active and tsunamigenic.

273  
274 Although we show no direct evidence that the ABfz uplifted during the GAE, the convergence of  
275 three back-projected travel time contours from our tsunami analysis lies just beyond the edge  
276 of the continental shelf (Figure 2). Another notable convergence lies at an identified scarp along  
277 the ABfz (Figure 2; discussion below). Although we favor the KSfz tsunami source, our analysis  
278 does not preclude co-rupture or later travel times from other sources. Indeed, assuming  
279 horizontal motion from the wedge slope, Suleimani and Freymueller (2020) identified the  
280 region near the continental shelf break as a likely tsunami source in 1964. Potential errors in  
281 the tabulated travel times (e.g., personal eyewitness accounts, timing) may point to inaccurate  
282 back-propagated locations for some of the observations. That being said, we do not see  
283 compelling evidence for the GAE first arrival tsunami source along the ABfz, but we will discuss  
284 a scarp and fault that is consistent with post-glacial Holocene uplift along the ABfz, closer to the  
285 Suleimani and Freymueller (2020) tsunami source region (see GAE tsunami source).

#### 286 287 **KODIAK SHELF FAULTS**

288 To characterize Neogene and younger slip on the KSfz, we present a compilation of vintage and  
289 modern active-source seismic profiles that cross sea floor scarps (Figure 4). Given a 30 to 50 m  
290 up-to-the-north seafloor scarp near our tsunami travel-time convergence region (Figure 3), and  
291 that these KSfz-related scarps presumably developed over the past ~13.5 kya (Carver et al.,  
292 2008), we infer a long-term uplift rate of 2.2 to 3.7 mm/yr. If we assume (1) that the faults  
293 coseismically slip only during  $M > 8$  ruptures, and (2) that they have a recurrence interval of 400  
294 years (i.e., 34 post-LGM earthquakes; Shennan et al., 2018), we would expect 1.4 to 2.3 m of

295 uplift per M8+ earthquake along this fault. As our tsunami analysis suggests focused uplift in  
 296 1964, then the slip-per-earthquake and per-fault must be greater than the long-term average  
 297 slip to produce multiple pronounced scarps related to the KSfz. Furthermore, the 8-m uplift  
 298 observed along the Patton Bay fault during the GAE (Plafker, 1969) suggests higher focused  
 299 uplift is possible, and likely, to produce such fault scarps.  
 300



301  
 302 **Figure 3.** Kodiak Island Shelf zone and related faults. a) 24-arc second global bathymetry data  
 303 with 100 m depth bathymetric contour. The map shows prominent NE-SW trending lineations  
 304 belonging to the KSfz. Arrows identify prominent KSfz seafloor scarps. Labeled are seismic profiles  
 305 (gray lines) and portions of the profiles presented in Figure 4 (white lines). The spatial location of  
 306 Figure 3b is denoted by the dashed line whereas Figure 5 is denoted by a dotted line. b) 8 arc-sec  
 307 bathymetry data in the dashed area of (a) showing ~20 m high Ugak and related faults highlighted  
 308 with the seismic profiles. Gray region indicates land. Star represents our preferred 1964 tsunami  
 309 source location.

310  
 311  
 312

313

314 **Seismic Reflection Profiling**

315 Our seismic reflection dataset to characterize the KSfz consists of legacy 24-channel airgun  
316 seismic reflection profiles acquired in 1975 from the former Mineral Management Services of  
317 Alaska (MMS), a sparker seismic profile collected by the MMS in 1976, a chirp seismic profile  
318 acquired in 2018, and a sparker profile acquired in 2015 (Figure 4). The legacy seismic profiles  
319 were obtained as digital scans of stacked travel time images from MMS permit 75-02 (Liberty,  
320 2013). The 2018 sub-bottom chirp data were provided to us from the Alaska Amphibious  
321 Community Seismic Experiment (Barcheck et al., 2020) and the 2015 sparker data were  
322 acquired using a 12-channel 500-Joule sparker seismic data on the US Geological Survey RV  
323 Alaskan Gyre (Liberty and Ramos, 2016). We migrate and depth convert the airgun images using  
324 stacking velocity values provided with the MMS image scans. We depth convert the chirp and  
325 sparker data using a velocity of 1,500 m/s. We interpret the seismic reflection data and show  
326 faults that offset the seafloor. We begin our analysis with seismic profiles that cross our  
327 inferred 1964 tsunami source, then explore profiles northeast and southwest of the tsunami  
328 source region.

329

330 *MMS line 484*

331 Our back-projection model places the GAE tsunami source location along a northeast-trending  
332 scarp close to MMS line 484 within the Kiliuda trough (Figure 3). Although this seismic profile is  
333 low resolution (approximately 35 Hz center frequency or a 40 m predominant wavelength), we  
334 note a 3.5-km-wide zone (CDP 145 – 180) where the seafloor is elevated about 50 m compared  
335 to the surrounding regions (Figure 4). At CDP 140 and CDP 180, we note both truncated and  
336 offset reflectors that increase in offset with depth, consistent with fault growth (Figure 4d). We  
337 term the fault at CDP 180 the Ugak fault, as this feature is located offshore of Ugak Island.  
338 Based on the proximity to the convergence of tsunami travel time contours, we interpret  
339 coseismic uplift on this fault as the first-arrival source for the 1964 tsunami that inundated  
340 several locations on the Kodiak Islands. The seafloor lineation associated with this fault extends  
341 at least 80 km (Figure 3), suggesting that an independent rupture would be capable of  
342 generating a M7 earthquake (e.g., Wells and Coppersmith, 1994). We interpret the fault that  
343 surfaces near CDP 140 (fault A, Figure 4d) as a south-dipping back thrust of the Ugak fault that  
344 controls the northern margin of the upthrown block. It is also possible that fault A moved in  
345 1964. The mottled seismic character and rugged seafloor topography within the uplifted  
346 seafloor region (CDP 140 to CDP 180) is consistent with deformed Cenozoic strata below the  
347 seafloor, similar to that mapped on the Kodiak Islands (Figure 4d; Moore et al., 1983). The

348 parallel reflectors and smooth seafloor topography to the south of the Ugak fault is consistent  
349 with late-Quaternary to Holocene marine strata. Here, we interpret a strong-amplitude,  
350 seafloor-parallel reflector as the base of modern deposition. Our interpretation is consistent  
351 with a regional unconformity that was seismically mapped beneath PWS and the Gulf of Alaska,  
352 which likely defines the onset of post-glacial sedimentation (i.e., Carlson and Molnia, 1975;  
353 Liberty et al., 2013; Finn et al., 2015; Haeussler et al., 2015; Liberty et al., 2019). We observe  
354 differentially offset reflectors across the Ugak fault and farther south, suggesting that additional  
355 faults near CDP 200 (fault B) and CDP 235 (fault C) have been Neogene-active (Figure 4d).  
356 Although poorly constrained, we estimate a fault dip of 70 to 80 degrees for the north-dipping  
357 faults. This dip is similar to the near surface expression of megathrust splay faults mapped near  
358 Montague Island (e.g., Plafker, 1969; Liberty et al. 2013; 2019). Using Hayes et al. (2018) Slab2  
359 geometry and assuming simple planar or listric fault geometry, we project the Ugak fault to  
360 splay from the megathrust at ~30 km depth beneath the Kodiak Islands.

361  
362 Faults B and C bound a 2-km-wide anticline and likely converge at about two to three km depth  
363 (Figure 4d). The shallowest reflectors do not show measurable offset (upper 100 m below  
364 seafloor), suggesting that these faults may no longer be active, or measure low slip relative to  
365 sediment deposition rates. If the pattern of faulting observed on MMS 484 is characteristic of  
366 these fault zones, it may suggest that the majority of Holocene slip is focused on the more  
367 landward faults.

368  
369 *Sparker line 242*

370 About 5 km to the southwest of MMS 484 and still within the Kiliuda trough (Figure 3), sparker  
371 seismic profile 242 shows the shallow character of the Ugak fault (Figure 4e). In particular, this  
372 higher-resolution view (about a 1-m dominant wavelength) of the Ugak fault shows a 25 m  
373 seafloor scarp towards the northwest (Figure 4e). Here, we observe no modern deposition in  
374 the fault's hanging wall to the northwest (hard water bottom, no subbottom reflectivity), an  
375 erosion channel directly above the fault, and subparallel reflectors to the southeast of the fault  
376 that are consistent with Holocene strata. We observe a second, more moderate seafloor high  
377 that we interpret as the hanging wall of fault B (Figure 4e). While we observe no measurable  
378 seafloor offset on MMS 484 across fault B, here we measure a seafloor offset of about 5 m.  
379 Assuming these two features both represent fault B, we conclude that either this fault is still  
380 active and the legacy airgun profiles do not provide adequate resolution to image Holocene  
381 displacements, or the fault slip varies along strike. Although Fault C controls the south limb of  
382 an anticline on MMS 484, this fault on Sparker 242 shows little evidence for Holocene motion.

383

384 Assuming that the three identified faults along sparker profile 242 represent north-dipping  
385 thrust faults, subbottom reflectivity suggests sediment deposition is focused on the seaward or  
386 footwall side of each fault. At a deposition-rate of one mm/year (Carlson and  
387 Molnia 1975), two notable subbottom reflectors at approximately 5 and 10 m below the  
388 seafloor are consistent with early and mid-Holocene unconformities; the 10-m reflector  
389 represents the Pleistocene-Holocene boundary. Similar age unconformities were inferred from  
390 seismic profiles near the PWS region within the Gulf of Alaska (i.e., Liberty et al., 2013; Finn et  
391 al., 2015), thus we suggest that these unconformities are pervasive, regionally significant, and  
392 with detailed age controls, may be used to compare slip rates across subduction zone  
393 segments.

394

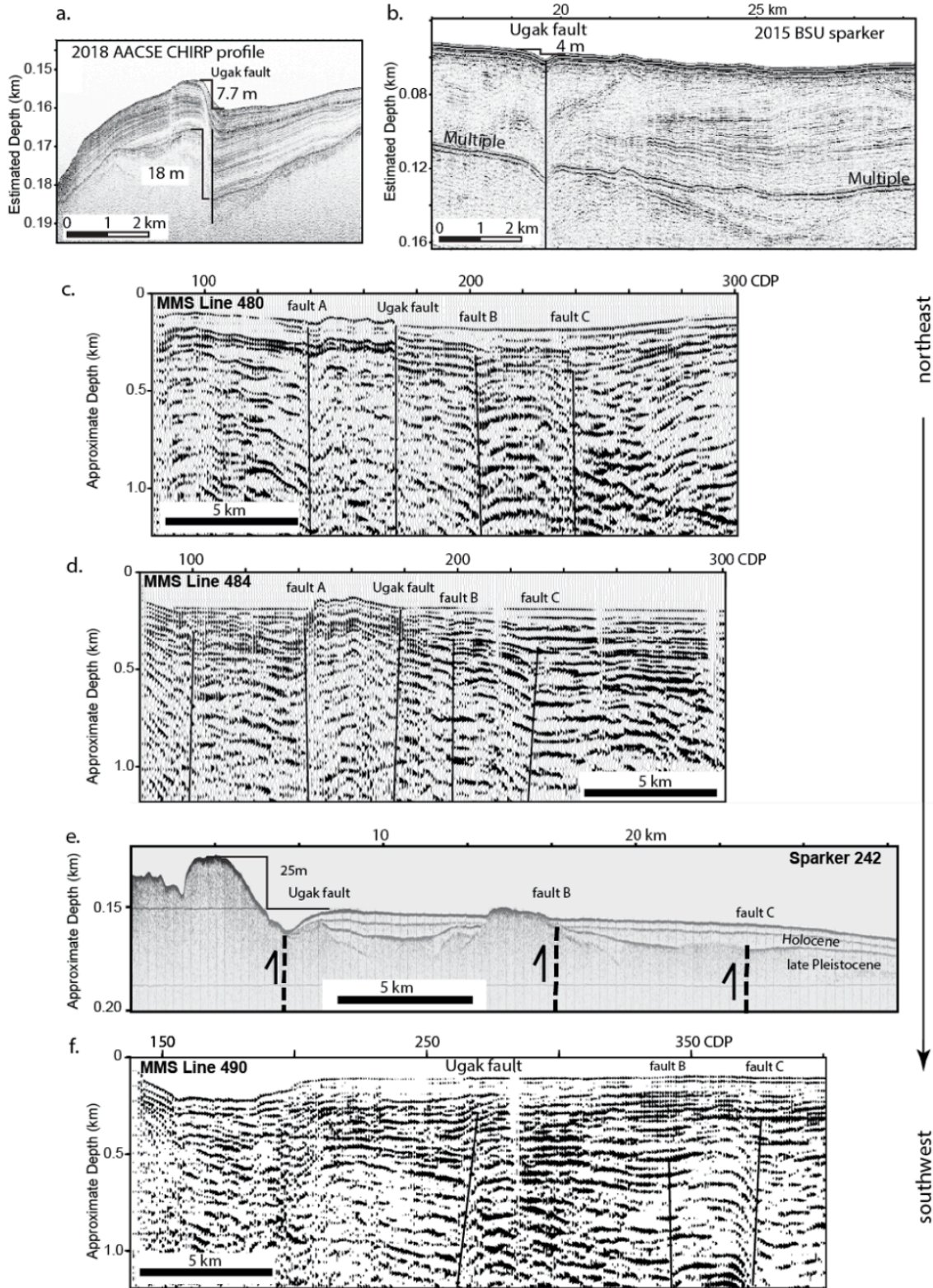
#### 395 *MMS line 490*

396 The northwest-southeast oriented MMS 490 is located 60 km to the southwest of MMS 484,  
397 outside of the Kiliuda depositional trough (Figure 3). To explore the southwest extension of  
398 active faulting, we trace sea floor scarps and examine the seismic character to identify the Ugak  
399 fault at CDP 270, fault B near CDP 345, and fault C near CDP 370 (Figure 4f). Here, based on  
400 reflector offsets, we measure a fault dip of about 65° to the north for the Ugak fault and fault C,  
401 and about 70° to the north for fault B. We observe that these faults show no measurable offset  
402 of reflectors above about 100 m depth, suggesting little Holocene fault motion. Faults B and C  
403 define the limbs of a four km wide fold with reflector offsets increasing with depth (Figure 4f).  
404 Small reflector offsets may indicate a back-thrust near CDP 200, but the convoluted reflection  
405 polarities preclude rigorous interpretation of this portion of the profile. The change in dip angle  
406 and reflector character on MMS 490 suggest reduced slip for this portion of the Ugak fault  
407 when compared to MMS 484.

408

#### 409 *MMS line 480*

410 Along MMS 480, located 20 km northeast of MMS 484, we identify the northeast extension of  
411 the Ugak fault as a 30-m-high seafloor scarp with the bathymetry data (Figure 3). Near CDP 170,  
412 we identify the Ugak fault from offset reflectors across a near vertical fault (Figure 4b). As with  
413 MMS 484 and MMS 490, we identify additional reflector offsets that we relate to faults A, B and  
414 C. MMS 480 lies within the Kiliuda trough, suggesting comparable deposition and/or erosion  
415 rates for MMS 484 and 480. We identify the greatest uplift of the Ugak fault closer to MMS 484.  
416 As with MMS 484 and MMS 490, MMS 480 shows a 4-km-wide anticline with no measurable  
417 sea floor offset (Figure 4b). Here, this anticline is approximately twice the width when



419 **Figure 4.** [Previous page figure caption]. Chirp (a, b), MMS (c, d, f), and sparker (e) seismic  
420 reflection profiles that cross the Ugak fault. Locations are noted on Figure 3. Seismic reflection  
421 profiles show variable along-strike changes in Ugak fault scarp height (~4 – 25 m) which implies  
422 different levels of post-LGM fault activity. Clear seafloor offset disappears by MMS 490 (f), which  
423 is 25 km SW of Sparker line 242 (e). Profiles are oriented from northwest to southeast (left to  
424 right) and shown from northeast to southwest. Note that the vertical and horizontal spatial scales  
425 in a, b and e (CHIRP, sparker reflection lines) differ from c, d and f (MMS reflection lines).

426  
427

428 compared to MMS 484, consistent with oblique shortening away from the presumed tsunami  
429 source. This fault divergence was also observed near the focus of GAE uplift along the Patton  
430 Bay fault system (Liberty et al., 2019), suggesting that more detailed fault mapping is needed to  
431 improve our understanding of fault kinematics within the KSfz.

432

#### 433 AACSE Chiniak Trough Chirp profile

434 Approximately 80 km to the northeast of the Kiliuda trough, we identify another cross glacial  
435 sediment trap termed the Chiniak trough (Figure 3). Here, a 3.5 kHz Chirp reflection profile  
436 acquired on the RV Sikuliaq in 2018 captures a robust post-glacial sediment record (Figure 4a).  
437 Along strike of the Ugak fault, we identify a 7.7 m sea floor scarp. Here, we measure a vertical  
438 offset of 18 m across a strong amplitude reflector that lies at the base of a package of  
439 subparallel reflectors that we presume are related to Holocene deposition (Figure 4a). From the  
440 assumption of a 13.5 ka age basal marker, we estimate an average Holocene deposition rate of  
441 about 1.5 mm/year to the south of the Ugak fault, with a decrease in deposition rate to the  
442 north and south away from the fault. Assuming the offset on the interpreted post-LGM surface  
443 represents the Holocene slip rate, we estimate an uplift rate of about 1.3 mm/yr. This  
444 represents an uplift rate of about 25% of that observed along sparker profile 242 and MMS 484.

445

#### 446 BSU Sparker profile

447 During 2015, we acquired a 500 J sparker seismic profile with a 12-channel hydrophone array  
448 across the northeast extension of the Ugak fault (Figure 3); termed BSU sparker profile (Liberty  
449 and Ramos, 2016). This profile lies about 20 km to the north of the Chiniak trough sediment  
450 trap. Here, the latest bathymetric survey dates back to 1933, so it is unclear from sea floor data  
451 alone as to whether tectonic scarps are present. On the BSU sparker profile, our largest sea  
452 floor displacement that lies along-strike of the KSfz measures four meters (Figure 4b). Across  
453 this scarp, we measure dipping reflectors in the upper tens of meters that are consistent with  
454 Quaternary fault motion. Although we identify no parallel reflectors that would point to



455 Holocene deposition, we identify a reflection pattern that is consistent with some motion on  
456 the Ugak fault. With a diminished offset of the sea floor scarp compared to our seismic profiles  
457 to the southwest, we suggest that this profile shows where the KSfz becomes less active. We  
458 note that trench-perpendicular structures have been mapped to the northeast of this profile  
459 location, coincident with the presumed boundary between the Kodiak and Kenai segments  
460 (Figure 1; Fisher, 1980; Fisher and von Huene, 1980).

461

#### 462 **Summary of KSfz**

463 From seismic and bathymetric data, we underscore two points. First, we note a divergence in  
464 distance between the Ugak fault and faults mapped to the south, consistent with oblique  
465 tectonic shortening along the KSfz. Second, the Ugak fault shows a maximum sea floor  
466 displacement along MMS 484 with diminished offset to the northeast and southwest. This may  
467 suggest a repeated tsunami source near the Kiliuda trough. Regardless if the Kiliuda trough may  
468 be a focus of exhumation, along strike sea floor scarps point to other tsunami sources that have  
469 likely inundated the Kodiak Islands during past earthquakes.

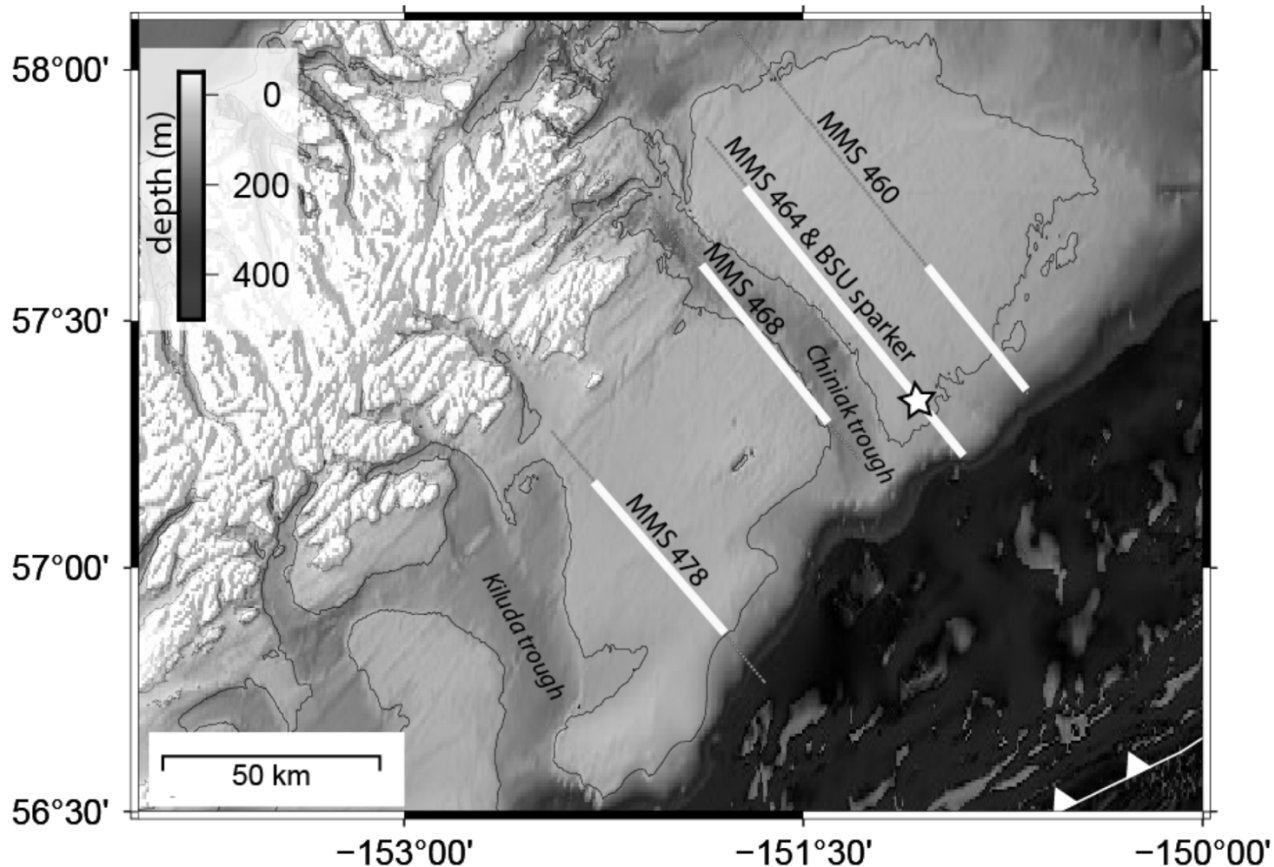
470

471 Scarp heights measure higher on the seismic profiles when subparallel faults have separation  
472 distances of 5 km or less (Figure 4). This might suggest that over a 20-30 km along-strike  
473 distance, there are changes along the decollement that favor closer splay fault separation and  
474 higher uplift rates. MMS 484 shows minor folding northwest of the Ugak fault, whereas  
475 reflectors on MMS 490 are relatively undeformed and continuous. Between faults B and C,  
476 however, reflectors suggest local shortening and growth faulting. These two faults merge at  
477 depth, consistent with a more complex upper plate structure when compared to a model  
478 where faults simply splay from the megathrust

479

480 Near Sitkinak Island (Figure 3), Zimmerman et al (2019) mapped two linear northwest-side-up  
481 scarps that they relate to the KSfz. The northwestern of the two scarps is 20–25 m tall and 29  
482 km long. The southeastern fault scarp, mapped only with single-beam bathymetry, may be  
483 upwards of 45 m tall and 80 km long. These observations imply that although the Ugak fault  
484 diminishes to the southwest, as mapped by MMS 490, the KSfz consists of many tsunamigenic  
485 faults whose interactions are poorly understood or constrained. This pattern differs from that  
486 observed along the offshore PWS faults, where a more focused exhumation region is observed  
487 (Haeussler et al., 2015; Liberty et al., 2019).

488



489  
 490 **Figure 5.** 24-arc second bathymetry across the Kodiak shelf detailing the Albatross Banks region  
 491 and select MMS seismic profiles. Portions of the seismic profiles highlighted on Figure 6 are shown  
 492 in white. The star represents a 16-m-tall scarp identified with MMS line 464 airgun and BSU  
 493 sparker profiles. This is a possible tsunami source, consistent with Kodiak City and Cape Chiniak  
 494 tsunami travel times.

495  
 496 In summary, we find the ~200 km long KSfz contains variable scarp heights and along-strike  
 497 variation in faulting style, although it is a long and laterally continuous structure. Large changes  
 498 in seafloor scarp height and evidence for tsunami generation along the fault zone in 1964 argue  
 499 for repeated, discrete KSfz uplift during megathrust slip, which translates to a high  
 500 tsunamigenic fault hazard at distances close to populated areas. We presume that the KSfz  
 501 splays from the megathrust near the southeastern limits of the Kodiak Islands. Coupled with  
 502 onshore faults that indicate sinistral slip (e.g., Carver et al., 2008), the KSfz is a complex  
 503 contractional fault system, which is possibly transpressional. Our observations warrant  
 504 additional paleoseismic investigations. More detailed bathymetric and seismic mapping is

505 needed to fully characterize the fault slip, interaction with the megathrust, and seismic hazard  
506 for this fault system.

507

#### 508 **ALBATROSS BANKS FAULT ZONE**

509 The 250-km long, 40-50 km wide northeast-trending ABfz lies within the Kodiak forearc and  
510 contains a series of southeast-verging thrusts, reverse faults, and anticlinal structures that lie  
511 near the continental shelf edge (Fisher, 1980; Fisher and von Huene, 1980; von Huene et al.,  
512 1980; Figure 3). These faults bound a number of forearc basins, and each likely splay from the  
513 plate boundary at 20-30 km depth (Moore et al., 1991). Because only single beam bathymetry  
514 data characterize the region surrounding the ABfz (NOAA National Centers for Environmental  
515 Information, 2004; Zimmerman et al., 2019), we present sparker and legacy airgun seismic  
516 profiles that constrain forearc structure and identify a possible tsunamigenic source.

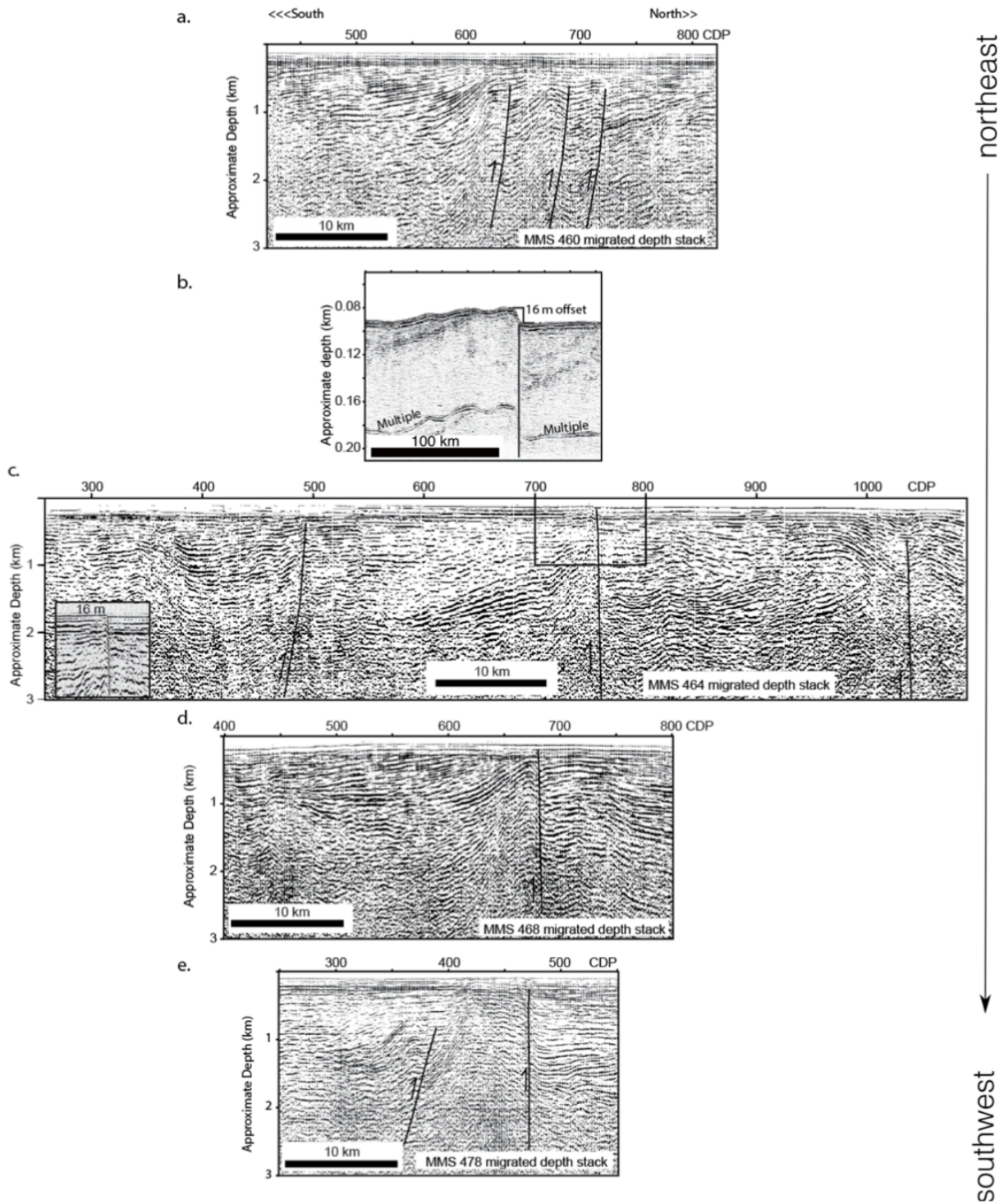
517

518 From the low resolution 24 arc-second bathymetry dataset, we do not identify seafloor scarps  
519 near the shelf-break that are similar in magnitude and length to the KSfz (Figure 5). The few  
520 multi-beam tracks that pass through this area point to a single seafloor uplift that we explore  
521 here. Our initial bathymetric assessment, coupled with seismic results of Fisher (1980) and  
522 Fisher and von Huene (1980) is consistent with 1) a majority of Holocene fault motion, as  
523 observed on the seafloor, being accommodated around the KSfz and 2) that the currently  
524 available low-resolution bathymetry cannot capture the full seafloor expression of the ABfz. In  
525 other words, there are likely other sea floor scarps along the ABfz that we have yet to identify.  
526 These possibilities are examined in greater detail with seismic profiles.

527

#### 528 ***GAE tsunami source***

529 We begin our discussion of the ABfz in the vicinity of a prominent fault scarp that we identify on  
530 MMS 464 and the coincident BSU sparker seismic profile (Figure 5, 6). This location is consistent  
531 with tsunami travel times from Kodiak City and Cape Chiniak (Figure 2). Had this location solely  
532 sourced a tsunami, Plafker (1969) would have measured an earlier arrival time from the Kalsin  
533 Bay station and later arrival times from the other stations farther to the southwest (Table 1).  
534 Given two tsunami sources, one from the Ugak fault and one from this scarp, Plafker (1969)  
535 would have still observed an earlier travel time from the Kalsin Bay station (Figure 2). Thus,  
536 assuming accurate tsunami arrival times, we conclude that the fault that lies beneath this scarp  
537 did not produce tsunamigenic uplift during the GAE. It is possible that the shelf slope region  
538 identified by Suleimani and Freymueller (2020) did produce a tsunami, but travel times from  
539 this location would have arrived later on all stations than what Plafker (1969) documented.



540  
541

542 **Figure 6.** [Figure caption for figure on previous page]. MMS airgun and sparker seismic reflection  
543 profiles of the Albatross Banks fault zone (ABfz). Sub-figures a, b, d and e show prominent splay  
544 faults that bound forearc basin structures, but do not appear to offset the seafloor. Sub-figure b,  
545 in contrast, shows a ~16-m high fault scarp that we imaged in 2015 with a sparker seismic source.  
546 We infer a Holocene slip-rate of 1.2 mm/yr for this particular fault.

547

548

549

550 *MMS line 464 and BSU sparker profile*

551 MMS 464 and the BSU sparker profile are coincident, lie immediately east of the Chiniak  
552 trough, and both cross the KSfz and ABfz (Figure 5). Where these profiles cross the ABfz, we  
553 measure about a 16 m sea floor scarp (Figure 6b, c). This scarp lies above a monocline that is  
554 consistent with the upper plate expression of a megathrust splay fault (e.g., Liberty et al., 2013;  
555 Figure 6c). We estimate a fault dip of about 80° on the shallow portion of this fault. The BSU  
556 sparker seismic profile shows south dipping strata and reflector truncations beneath the scarp  
557 (Figure 6b). Given the seismic character and location on the shallow shelf, we interpret the  
558 shallow stratigraphy as representing pre-Holocene strata. Thus, a robust Holocene slip rate  
559 estimate was not possible for this fault at this location. However, with the assumption that  
560 seafloor topography was reset during the LGM, this fault has likely been active during many  
561 Holocene earthquakes. Thus, we interpret this scarp as tsunamigenic. If the 16 m scarp  
562 developed only over the past 13.5 ka, we estimate a slip rate of 1.2 mm/year.

563

564 *MMS line 460*

565 MMS 460 is located near the transition from the Kenai to Kodiak segment, 20 km to the  
566 northeast of MMS 464 (Figures 1 and 5). The seismic profile shows asymmetric, km-scale  
567 folding bound by three faults between CDP 640 and 725 (Figure 6a). The distance between each  
568 ~70° SE dipping fault is less than 5 km and offset reflectors cannot be traced to the seafloor,  
569 implying relatively low Holocene slip rates. It is unclear how each of these faults relate to the  
570 presumed tsunamigenic fault highlighted on MMS 464, but the changing seismic character over  
571 a length scale of 20 km suggests that the ABfz is complex. The lack of a sea floor scarp suggests  
572 limited Holocene motion near the Kenai segment boundary.

573

574 *MMS line 468*

575 MMS profile 468, located 20 km to the southwest of MMS 464, crosses the Albatross Banks  
576 near the Chiniak trough (Figure 5). On this profile, we identify a single high-angle splay fault  
577 near CDP 685 that lies along strike of the tsunamigenic fault identified on MMS 464 (Figure 6d).

578 There is noticeable folding on the hanging-wall side of this presumed splay fault to less than  
579 300 m below the sea floor. The fault does not appear to offset the sea floor. This suggests that  
580 the tsunamigenic sea floor scarp is not regionally extensive and that focused uplift is restricted  
581 to a narrow region surrounding MMS 464.

582

#### 583 *MMS line 478*

584 MMS 478 lies between the Chiniak and Kiliuda troughs (Figure 5). We note a prominent  
585 anticline centered near CDP 440 whose axis trends northwest-southeast (Fisher and von Huene,  
586 1980; Figure 6e). We identify two high-angle splay faults on this profile that are separated by  
587 about 7 km. Folding is tighter across the northwest fault's hanging-wall (CDP 400) compared to  
588 the hanging wall of the fault at CDP 460 (Figure 6e). We observe no shallow offset stratigraphy  
589 across either fault, suggesting little to no Holocene motion.

590

#### 591 **Summary of ABfz**

592 Faults belonging to the ABfz are largely reverse faults originally mapped offshore Kodiak  
593 between Sitkinak Island to the southwest and the Kenai segment boundary to the northeast  
594 (von Huene et al., 1980; Figure 1 and 3). However, its near-surface architecture, Holocene  
595 activity, and along-strike extent are largely unknown. Limited and generally low-resolution  
596 bathymetry data for this region do not show conspicuous seafloor lineaments that we could  
597 interpret as Holocene fault scarps (Figure 2 and 3). But the seismic data allowed us to identify a  
598 16-m scarp that suggests recent tectonic activity. The MMS airgun seismic data do not have the  
599 resolution to image seafloor offsets less than about 10 m, and this underscores the need to use  
600 both high-resolution bathymetry and sparker seismic together to interpret fault activity.

601

#### 602 **KSfz AND ABfz COMPARISON**

603 Although our datasets are limited, we find that both the scarp height and morphology  
604 associated with the KSfz are much more prominent than those associated with the ABfz. Such  
605 an observation implies a majority of Holocene faulting has been accommodated closer to the  
606 Kodiak Islands shoreline (i.e., KSfz) rather than along faults nearer to the edge of the shelf (i.e.,  
607 ABfz). An increase in fault scarp height may indicate that through time, the location of focused  
608 deformation transitioned from the outer to inner wedge regions of the forearc, which is  
609 expressed in the higher uplift-rates of the KSfz compared to the ABfz we infer. One plausible  
610 hypothesis is that higher splay fault activity (exhumation) is a function of the where the wedge  
611 changes from mechanically weak (outer wedge) to strong (inner wedge backstop). In the PWS  
612 region, thermochronology and seismic reflection data show that a major splay fault separates

613 these regions (Haeussler et al., 2015; Liberty et al., 2013). Rocks accreted before and after the  
614 subduction of a spreading center in the Gulf of Alaska are similar in age between PWS and  
615 those onshore of the Kodiak Islands (Bradley et al., 2003). Different accretionary episodes form  
616 the strong-to-weak wedge transition and the location of the KSfz roughly coincides with this  
617 structural boundary. Alternatively, the deformation rates have always been higher within the  
618 KSfz than the ABfz, which is still consistent with differences in wedge mechanical strength. We  
619 conclude that the tsunamigenic fault hazard is concentrated in the near-shore region of the  
620 Kodiak Island, although the ABfz and slope regions are still capable of producing tsunamis.

621

#### 622 **UPPER PLATE AND PLATE BOUNDARY STRUCTURE**

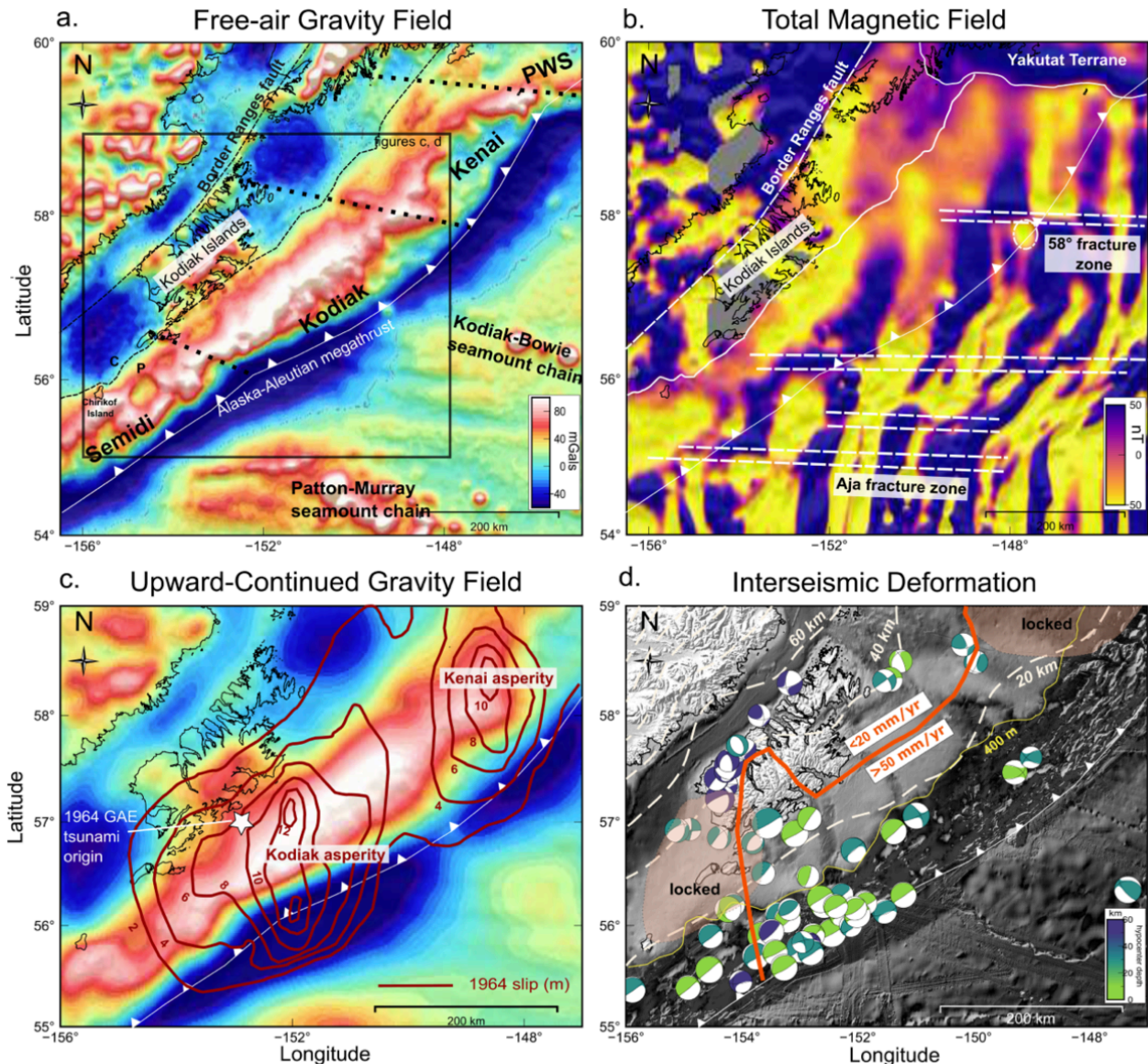
623 Gravity and magnetic data can reveal unique signals of subducting and upper plate structure.  
624 Despite the numerous studies that have uncovered correlations between moment-release,  
625 subducting structure, and down-dip rupture limits (e.g., Wells et al., 2003; Song and Simons,  
626 2003; Bassett and Watts, 2015), the Alaska subduction zone in particular seems to be more  
627 complex for understanding seismogenic behavior. A positive gravity anomaly dominates the  
628 Alaska forearc (Figure 7a) and this anomaly was interpreted by Wells et al. (2003) as resulting  
629 from a highly dense inner-wedge or duplexed structure near the plate interface. Seamounts  
630 and fracture zones on the Pacific plate offshore Kodiak are observed on gravity and magnetic  
631 data, but subducted expressions of these structures below the forearc are lacking (von Huene  
632 et al., 1999; Saltus et al., 1999; Mankhemthong et al., 2013; Figure 7a, b). Thus, the relationship  
633 between coseismic rupture, subducted topography, and upper plate splay faulting deserves  
634 further scrutiny for the Kodiak Islands region.

#### 635 **Gravity data**

636 Free-air gravity anomalies over subduction zones map density differences related to either  
637 plate interface or upper plate structures (Smith and Sandwell, 1997). The spatial distribution of  
638 the free-air gravity field over the North American and Pacific plates near the Kodiak Islands  
639 shows several regional tectonic features that may influence seismogenesis (Wells et al., 2003;  
640 Bassett and Watts, 2015). We apply upward-continuation and bandpass filtering to the free-air  
641 gravity field to constrain the extent and geometry of the accretionary prism and upper-crustal  
642 faulting (Figures 7 and 8).

643

644 The free-air gravity map of the Kodiak-Kenai Peninsula region helps to clarify relationships  
645 between rock units in the accretionary prism. The Border Ranges fault zone marks the contact  
646 between the Mesozoic and Cenozoic accretionary prism and its backstop (Fisher, 1981; Plafker  
647 et al., 1994; Pavlis and Roeske, 2007; Mankhemthong et al., 2013). This fault coincides with a



648  
 649 **Figure 7.** Geophysical expressions of crustal structure and segmentation across the western Gulf of  
 650 Alaska. a) Free-air gravity anomaly map (Sandwell et al., 2014). Dotted black lines signify segment  
 651 boundaries discussed in the text. Dashed black lines denote Border Ranges fault. Box denotes location of  
 652 c and d. b) Total magnetic field from the EMAG2 database (Meyer et al., 2017). Gray regions represent  
 653 data gaps. Solid white lines signify terrane boundaries. Major fracture zones (dashed white lines) from  
 654 Naugler and Wageman (1973) are revealed as offset magnetic lineations. Note that several fracture  
 655 zones (e.g., 58° fracture zone, Aja fracture zone) appear landward of the trench. c) Upward-continued  
 656 free-air gravity anomaly to a height of 10 km. Superposed are coseismic 1964 slip-contours (2 m) of  
 657 Ichinose et al., (2007). We observe that slip was confined mostly to the positive gravity anomaly regions.



658 *d) Seafloor bathymetry map with post-1964 earthquakes ( $M > 5$ ) colored by hypocenter depth and plate*  
659 *locking model from Zweck et al., (2002). The 400 m bathymetry contour (yellow) delimits the continental*  
660 *shelf-break. The bold orange line signifies a major change in the slip-rate deficit as derived from geodetic*  
661 *inversion analysis (Li et al., 2016). Focal mechanisms from the CMT catalog (1976-2016) show the along-*  
662 *strike contrast in interseismic stress release following the GAE for the Kodiak region. Off-white dashed*  
663 *lines show the depth to the plate interface in 20 km intervals from the Slab2 model (Hayes et al., 2018).*  
664

665

666 conspicuous gravity lineament that bounds the northwest extent of the Kodiak Islands (Figure  
667 7a). To the southeast of the Kodiak Islands, a northwest to southeast transition from low to  
668 high gravity signals forms a lineation that defines the boundary between the older “Chugach  
669 terrane” part of the accretionary prism, and the younger Paleocene-Eocene “Prince William  
670 terrane” (Burns, 1985; Plafker et al., 1994; Wells et al., 2003). These two terranes are  
671 considered to divide the accretionary complex (Plafker et al., 1994), but the upper plate across  
672 this boundary consists of no discernable density contrast. Instead, this anomaly has been  
673 interpreted to stem from duplexing or other crustal densification processes near the plate  
674 boundary (Wells et al., 2003; Mankhemthong et al., 2013). In addition, significant rock uplift of  
675 the accretionary complex has brought higher velocity and presumably denser rocks closer to  
676 the surface. This regional exhumation process might also explain the source of the positive  
677 gravity anomaly (Ye et al., 1997) that may structurally link the KSfz and Patton Bay fault systems  
678 (Figure 7, 8). Of note is that the related gravity lineation extends across segment boundaries  
679 where sea floor scarps and active faults have not been mapped.

680

681 We observe two circular gravity lows that bound the Kodiak Islands to the northeast and  
682 southwest, which were first noted by Wells et al. (2003) (Figure 7). These ~120 km wide low  
683 gravity regions lie between the Border Ranges fault zone to the north and the Prince William  
684 terrane boundary to the south. The limits of these gravity lows also coincide with our mapped  
685 extent of the KSfz (von Huene et al., 1980). The observed correlation between positive gravity  
686 anomalies and active splay faults suggests that offshore faults within the Prince William terrane  
687 (i.e., KSfz, ABfz) may have higher slip rates compared to faults closer to mainland Alaska.

688

689 Ye et al. (1997) identified a low seismic velocity mid-crustal body that spatially matches the  
690 large northern gravity low between the Kodiak Islands and Kenai Peninsula. This gravity/seismic  
691 velocity low could be evidence for large-scale underplating of subducted sediment or a  
692 seamount as proposed by Ye et al (1997) and Mankhemthong et al (2013). The oblate negative  
693 gravity anomaly to the southwest of the Kodiak Islands does not correlate with any previously

694 suggested upper plate (mid- to lower-crustal) source (Figure 7 and 8). The upper Miocene to  
695 Quaternary Tugidak basin has been mapped on Chirikof and part of the Trinity Islands, but this  
696 shallow basin may not account for the observed gravity low. Similar to the gravity anomaly that  
697 bounds the northeast side of the Kodiak Islands, we hypothesize that lower crustal underplating  
698 may be the source of this anomaly, as this feature persists even on the filtered long-wavelength  
699 component of the free-air gravity field (Figure 8).

700

701 Our examination of the gravity data does not further constrain this interpretation, however the  
702 spatial relationship between these two gravity lows that sandwich the high elevation Kodiak  
703 Islands may link underplated regions to lower exhumation rates. Moreover, the northeastern  
704 gravity low appears to correlate with our current understanding of subduction zone  
705 segmentation, and it correlates with a region of high slip-rate deficit outlined by Li et al. (2016)  
706 (Figures 7 and 8).

707

708 Farther southwest along the Semidi segment, the negative gravity anomaly becomes positive  
709 (Wells et al., 2003). This observation indicates a different crustal character between subduction  
710 zone segments. Few crustal seismic reflection data exist across this region (e.g., Becel et al.,  
711 2017). Robust forward potential field modeling of additional crustal-scale seismic reflection  
712 data may be needed to assess underplating as a possible tectonic mechanism. If underplating is  
713 occurring both northeast and southwest of the Kodiak Islands, this stresses the importance of  
714 interface processes controlling splay fault activation and megathrust segmentation.

715

### 716 **Magnetic data**

717 The total-magnetic field around the Kodiak Islands highlights several distinct tectonic structures  
718 on the upper plate and topography on the incoming Pacific plate (Figure 7b). Some of these  
719 continuous or offset magnetic lineations correspond to inferred earthquake segment  
720 boundaries (von Huene et al., 1999; von Huene et al., 2012). In particular, the total magnetic  
721 field shows offsets of the oceanic plate magnetic stripes that are most likely sourced by fracture  
722 zones (Naugler and Wageman, 1973). The pattern of magnetic stripes is continuous across the  
723 trench, showing that incoming plate structures are imaged below the accretionary wedge and  
724 outer forearc (Figure 7b). Offset magnetic lineations on the incoming Pacific plate reveal at  
725 least four main fracture zones that are presently subducting near, and beneath, the Kodiak  
726 Islands. The Aja and two unnamed fracture zones are observed south of 57° N latitude. A  
727 magnetic lineation related to the 58°N fracture zone persists almost to 200 km northwestward  
728 of the trench, down to a plate interface depth of ~20 km (Hayes et al., 2018). This lineation lies

729 at the inferred northeast boundary of the Kodiak subduction zone segment (von Huene et al.,  
730 1999; von Huene et al., 2012; Shennan et al., 2014). We note that although the KSfz lies  
731 between the landward extension of the 58° N and Aja fracture zones, these features have  
732 presumably migrated northwest with plate motions and there may be no relationship with the  
733 lateral extent of the KSfz (Figure 7).

734

735 Both the Chugach and Prince William terrane boundary (seaward of the Kodiak Islands) are  
736 revealed by magnetic field gradients, where the total-field switches from positive to negative  
737 (Figure 7b). We consider magnetic anomalies to be features in the total magnetic field data that  
738 disrupt the otherwise contiguous nature of upper plate magnetic signatures. A majority of both  
739 the Chugach and Prince William terranes are characterized by negative total-field magnetic  
740 anomalies, as expected of accreted sediments that contain little to no magnetically susceptible  
741 minerals (Blakely, 1996; Saltus et al., 2007). Furthermore, this negative magnetic anomaly is  
742 clearly bound by the Border Ranges fault system to the northwest; the northern region of the  
743 magnetic domain of the Border Ranges fault has been referred to as the 'Knik Arm' anomaly  
744 (Grants et al., 1963). In the northern Gulf of Alaska, the southern limit of the Yakutat terrane is  
745 highlighted by a linear magnetic high anomaly that also coincides with the presumed  
746 southwestern PWS segment boundary asperity (Bruns, 1983; Brocher et al., 1994). The major  
747 magnetic domains evident on the upper plate are the southern Alaska magnetic high and the  
748 Chugach magnetic low which are sourced from dense lower crustal mafic and upper crustal  
749 sedimentary rocks, respectively (Saltus et al., 2007).

750

751

#### 752 **RELATIONSHIPS BETWEEN FAULTING, SUBDUCTING STRUCTURE, AND LOWER CRUSTAL DEFORMATION**

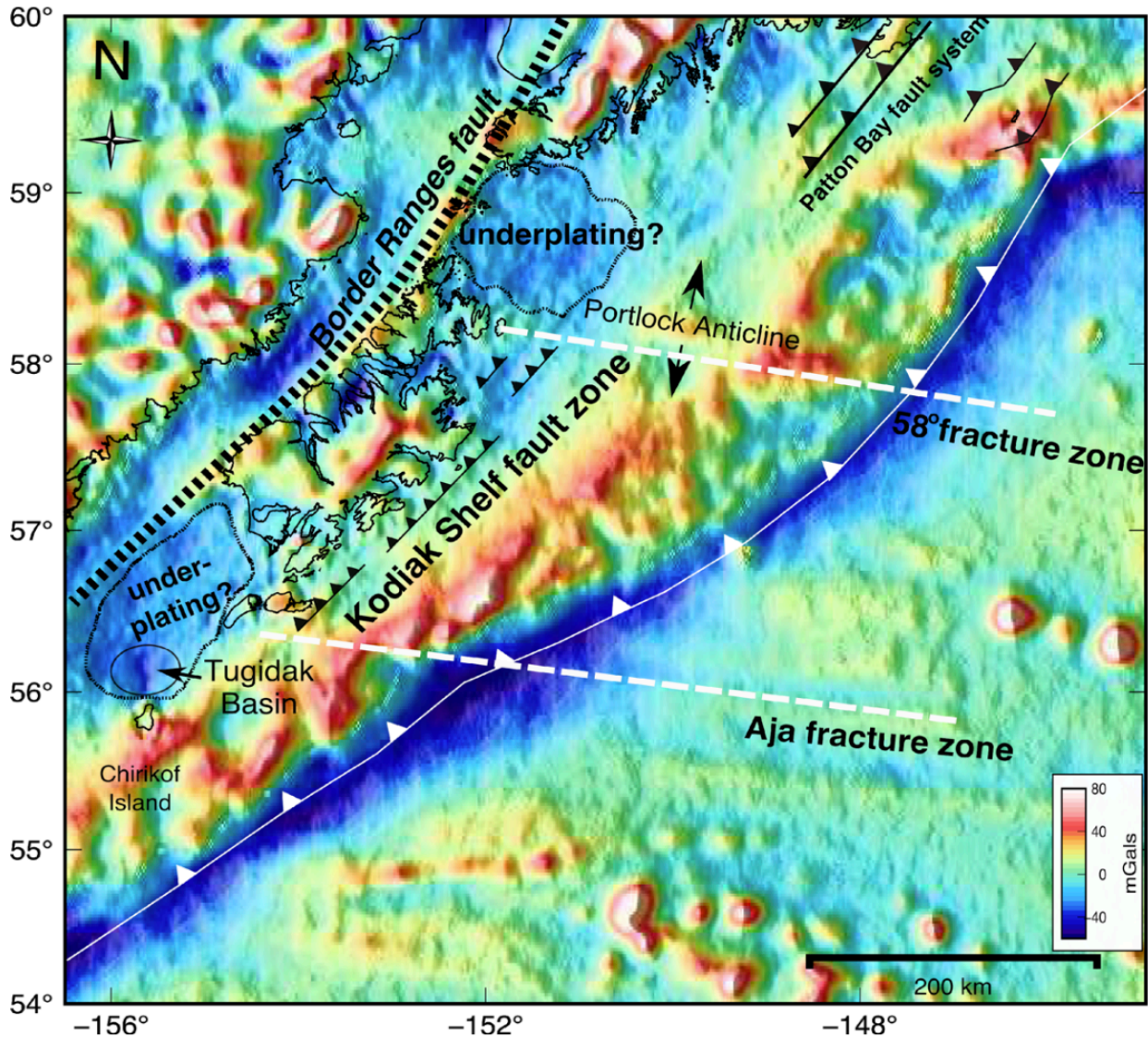
753 In order to relate structural controls of segmentation and subducting plate influences to upper  
754 plate deformation across the Kodiak region, we compare 1964 earthquake slip models to  
755 potential field and post-1964 seismicity and geodesy data (Figure 7c). Coseismic models from  
756 the 1964 earthquake reveal three main slip-patches, or asperities, from joint inversions of  
757 geodetic, seismic, and tsunami data (Johnson et al., 1996; Ichinose et al., 2007). The  
758 southwestern, or Kodiak asperity, with 10 to 12 m slip, was focused below the shallow forearc  
759 with down-dip rupture generally not extending across the Prince William terrane boundary  
760 (Ichinose et al., 2007). The second asperity lies offshore the Kenai Peninsula and northeast of  
761 the Kodiak Islands (von Huene et al., 1980; Ichinose et al., 2007). We refer to this ~100-km-wide  
762 slip concentration as the Kenai asperity (Cohen and Freymueller, 2004; Kelsey et al., 2015).  
763 When we upward continue the free-air gravity field to a height of 10 km, the resultant low-pass

764 gravity field shows that the high-slip regions of both the Kodiak and Kenai asperities are within  
765 the positive gravity region (Figure 7c). We note that this particular slip inversion had limited  
766 azimuthal seismic station coverage and inversion resolution is dependent upon three different  
767 datasets (Ichinose et al., 2007). In general, forearc basin depocenters (negative gravity  
768 anomalies) correlate with asperity location (e.g., Song and Simons, 2003; Wells et al., 2003),  
769 however, here it does not, as previously noted for the Alaska-Aleutian subduction zone by Wells  
770 et al. (2003) and Ichinose et al., (2007).

771

772 The 58° fracture zone divides the 1964 GAE slip maxima of the Kodiak and Kenai asperity  
773 boundaries (Figure 7b, c). If this fracture zone is indeed a persistent segment boundary, the  
774 1964 earthquake either had enough energy to rupture across the 58° fracture zone or perhaps  
775 the fracture zone only halted rupture momentarily, as has been observed in the M8.4 Peru  
776 megathrust earthquake in 2001 (e.g., Robinson et al., 2006). Moreover, paleoseismic evidence  
777 indicates the Kodiak asperity sometimes ruptures with, or sometimes independently of, the  
778 Prince William Sound asperity (Shennan et al., 2014). Geodetic models show spatial  
779 distributions of interseismic locking are different from coseismic strain release (Zweck et al.,  
780 2002; Suito and Freymueller, 2008; Li et al., 2016). The 58° fracture zone does not show a  
781 strong gravity signal on the incoming Pacific plate, which is likely due to 2 - 3 km of low-density  
782 sediment subducting beneath the trench (Reece et al., 2011; von Huene et al., 2012; Gulick et  
783 al., 2015; Figure 7a). The E-W magnetic lineament traces the 58° fracture zone beneath the  
784 Pacific plate and an oblique N85°W trending (filtered) gravity anomaly coincides with this  
785 feature beneath the wedge (Figure 8). The gravity field records differences in density due to  
786 structural juxtapositions in upper plate deformation, which is probably driven by oblique  
787 convergence of the subducting Pacific plate. Fracture zone morphology is typified by a large  
788 ridge and trough structure that remains structurally competent as it spreads from the mid-  
789 ocean ridge and into the subduction zone (Menard and Atwater, 1969; Sandwell, 1984). The  
790 outer wedge of subduction zones is the mechanically weaker portion of the subduction zone  
791 forearc (Wang and Hu, 2006; Noda, 2016). Wedges thus record recent and current deformation  
792 of subducting high-relief from the incoming plate, such as seamounts or fracture zones (Basset  
793 et al., 2015). Considering both fracture zone morphology and constraints from both potential  
794 field datasets, we interpret the N85°W trending feature to be the upper plate expression of the  
795 subducted 58° fracture zone below the outer wedge. Furthermore, a concentric anomaly in the  
796 total magnetic-field near the trench suggests a subducted seamount may be associated with  
797 the 58° fracture zone (Figure 7b; Fruehn et al., 1999; von Huene et al., 2012).

798



799  
 800 **Figure 8.** Low-pass filtered free-air gravity map for the Gulf of Alaska region. This map is filtered to  
 801 remove signals with wavelengths greater than 100 km and illuminated from the southeast to highlight  
 802 gravity lineaments related to forearc splay faults and terrane boundaries. Note the continuity of the  
 803 Kodiak Shelf fault zone and its gravity expression diminishes seaward of the Alaska forearc. Splay  
 804 faults belonging to the Patton Bay fault system are also highlighted further to the north on the PWS  
 805 segment. The gravity signature of the subducted 58° fracture zone within the wedge and its upper  
 806 plate structural expression (Portlock Anticline) share the same N85W oblique trend. Two prominent  
 807 low gravity anomalies south and north of the Kodiak Islands are interpreted as possible sites of  
 808 underplating. Note these two gravity lows bound both the mapped KSfz and the projection of  
 809 subducted 58° and Aja fracture zones (white dashed lines).

810 The Kodiak segment transitions from strongly to moderately locked below the Trinity Islands  
811 and northeast Kodiak Island (Figure 7d). This is in contrast to that observed with the PWS  
812 segment, which is completely locked (Zweck et al., 2002; Sauber et al., 2006; Freymueller et al.,  
813 2008). The gravity boundary between the Tugidak basin low and the higher values of Kodiak  
814 Island are potential fields expression of this rupture boundary (Figure 7a). Moreover, lower  
815 plate conditions change along the Gulf Alaska from PWS to the Kodiak Islands. For instance, the  
816 trailing edge of the Yakutat terrane (Figure 7b) is highly coupled to the Pacific plate (Brocher et  
817 al., 1994; Zweck et al., 2002). These structures together have much shallower dip ( $\sim 4^\circ$ ) when  
818 compared to the Kodiak region, where the dip gradually steepens to  $\sim 10^\circ$  (Brocher et al., 1994;  
819 Eberhart-Phillips et al., 2006; Sauber et al., 2006; Hayes et al., 2018). Roughness of the  
820 subducting Pacific plate could also influence regional variations in coupling because there are  
821 numerous seamounts and fracture zones sitting offshore from the Kodiak Islands, as shown in  
822 the potential fields data.

823  
824 Post-1964 seismicity varies along-strike across the Kodiak Islands (Figure 7d). There is a relative  
825 paucity of large earthquakes ( $M > 5$ ) for the northeast region and a majority of the seismicity is  
826 occurring offshore and southwest of the Kodiak Islands, suggested by others to have occurred  
827 in the subducting Pacific plate (Doser et al, 2002; Doser, 2005). Focal mechanisms in the  
828 southwest Kodiak region are consistent with thrust faulting where the hypocenters cluster  
829 between 20 to 40 km depth. Models suggest the megathrust is mostly locked landward of these  
830 moderate seismic events (Zweck et al., 2002). However, shallow thrust events coupled with  
831 significant margin erosion, which may cause a shallowing of the slope angle, suggests that the  
832 southwest region of Kodiak may be in the underthrusting phase of the accretionary cycle  
833 (Gutscher et al., 1998). Underthrusting focused beneath the shelf may be accommodating some  
834 interseismic slip and may provide a means to maintain down-dip locking below southwest  
835 Kodiak. A lack of underthrusting near the plate interface may also explain why the KSfz tapers  
836 out across the Semidi segment.

837

### 838 ***Semidi/Kodiak segment boundary***

839 Rupture models for a 1788 A.D., a 1440-1620 A.D., and a 1060-1110 A.D. earthquake recognize  
840 a semi-persistent boundary near the Trinity Islands (Briggs et al., 2014; Shennan et al., 2014;  
841 Kelsey et al., 2015; Figure 3). The oblique subduction of fracture zones and seamount chains  
842 could complicate megathrust interface conditions, upper plate deformation, and could exert  
843 enough structural control to act as a segment boundary (von Huene et al., 2012). A pronounced  
844 gravity gradient parallels the KSfz. This lineament extends southwest of Chirokof Island and

845 northeast to the Portlock anticline (Figures 7 and 8). The gravity signature related to the KSfz  
846 terminates near the northern segment boundary, but a similar gravity signature does not define  
847 the Kodiak/Semidi segment transition. The related lineation may instead mark the location of  
848 the eroding continental shelf-break or alternatively, could represent older splay faults that do  
849 not offset the seafloor.

850

851 Observations from multi-channel seismic reflection data (ALEUT experiment) across the Semidi  
852 and Shumagin segments suggest that the hydration state of the megathrust and structure of  
853 the incoming plate play pivotal roles in regulating seismicity and fault formation (i.e., Li et al.,  
854 2015; Shillington et al., 2015; Li et al., 2018). Intermediate-depth earthquakes are more  
855 abundant across the Shumagin and Kodiak regions, suggesting the Semidi segment is in a  
856 different stage of the earthquake cycle (Shillington et al., 2015). In addition, these earthquakes  
857 may be below the continental Moho, but ray coverage is insufficient to image deeper  
858 megathrust structure in detail (Becel et al., 2017). Regarding upper plate structure, the central  
859 Semidi segment appears to have several high-angle splay faults within the outer wedge,  
860 seaward of the continental shelf break (Li et al., 2018). However, splay faults landward of the  
861 continental shelf-break are largely unknown on the Semidi segment (von Huene et al., 1987;  
862 von Huene et al., 2012). Pre-existing structural heterogeneity on the incoming plate can permit  
863 fluids to enter the subduction zone and increase the pore pressure, thereby reducing the  
864 effective normal stress and making it easier for earthquake rupture to propagate through this  
865 region, once initiated. This mechanism is inferred to be responsible for the greater number of  
866 intermediate depth earthquakes for the Shumagin and Kodiak segments (Shillington et al.,  
867 2015). Our results agree with this interpretation for the southwest Kodiak segment, especially  
868 because offset magnetic lineations in the oceanic crust (corresponding to fracture zones), when  
869 subducted at the trench, could contribute to fault-bending and be favorable to fluid permeation  
870 (Figure 7b).

871

### 872 ***Kodiak/Kenai segment boundary***

873 The northeastern boundary of the Kodiak segment has been inferred to exist somewhere  
874 between the northern Kodiak Islands and the Kenai Peninsula (e.g., von Huene et al., 2012).  
875 Although Johnson et al (1996) and Ichinose et al (2007) show an isolated 1964 slip patch  
876 between the PWS and Kodiak segments, only recently have geologic observations been made  
877 that suggest an independent Kenai segment (e.g., Hutchinson and Crowell, 2007; Shennan et al.,  
878 2014; Kelsey et al., 2015). If so, then it seems likely that there is some structural expression of  
879 the segment boundary between the Kodiak Islands and the Kenai Peninsula.

880

881 We have newly characterized the 58° fracture with magnetic and gravity data (Figures 7 and 8).  
882 A prominent structural high on the upper plate lies immediately above the subducted 58°  
883 fracture zone on the Kodiak forearc and sources the positive gravity lineament on the landward  
884 side of the continental shelf break (Figure 7; Fisher, 1980). The trend of both the related  
885 anticline and this fracture zone bound the negative gravity anomaly to the north of Kodiak  
886 Island (Figure 7a and 8). However, the uplift is Miocene to Pliocene in age (von Huene et al.,  
887 1987) and is most likely not associated with subduction of the 58° fracture zone as the depth to  
888 the plate interface is nearly 20 to 25 km below the anticline (Hayes et al., 2018). Northwest of  
889 the 58° fracture zone trend, however, KSfz scarp heights diminish and offset reflectors in MMS  
890 reflection profiles do not extend to the seafloor. KSfz scarps are not apparent onto the Kenai  
891 segment, which suggests the zone of focused uplift (i.e., active splay faulting) does not persist  
892 onto the negative gravity anomaly region (Figure 7a). Unfortunately, geodetic inversions lack  
893 resolution across the Kodiak/Kenai segment transition, as it lies sufficiently far offshore (Zweck  
894 et al., 2002; Freymueller et al., 2008; Li et al., 2016). The Ichinose et al. (2007) slip model shows  
895 that the middle asperity is confined to the Kenai Peninsula region and the 58° fracture zone  
896 forms a possible southern boundary (Figure 7c); though the influence of a subducted fracture  
897 zone is speculative. Thus, there is a structural (KSfz), geophysical (gravity, magnetics), and  
898 coseismic expression (slip model) of physical property changes that can be related to inferred  
899 plate interface conditions.

900

901 The Kodiak and Kenai segment boundary may also be driven by differences in subducting  
902 sediment volume. Between the 58° fracture zone and PWS, there is an absence of significant  
903 structural relief on the incoming plate and sediment from the Surveyor Fan is the primary  
904 material above the oceanic crust (Reece et al., 2011). Seismic reflection profiles show more  
905 than one km of sediment near the trench (Fruehn et al., 1999). Assuming enough of the  
906 Surveyor Fan has been subducted, this sediment may contribute to the low velocity anomaly,  
907 negative free-air gravity, and general lack of thrust earthquakes occurring near the interface  
908 below the Kenai Peninsula (Ye et al., 1997; Doser et al., 2002). Furthermore, geomechanical  
909 models of forearc basin growth and wedge dynamics show that if there is significant  
910 sedimentation on the upper plate, then pervasive internal deformation (i.e., faulting) in the  
911 forearc basin is not favored because the wedge becomes stable due to lower shear traction on  
912 the megathrust (Fuller et al., 2006).

913



914 Porto and Fitzenz (2016) adopted a Bayesian approach using earthquake catalog data to assess  
915 segment boundaries for the Alaska subduction zone. Their methodology suggests a potential  
916 segment boundary northeast of the Kodiak Islands. This is broadly consistent with the along-  
917 strike change in focal mechanism character (i.e Figure 7d) and where we interpret the  
918 northeast termination of the KSfz.

919

#### 920 **FAULT SEGMENT SUMMARY**

921 We infer from legacy seismic reflection data (MMS profiles) that the KSfz faults are splay faults  
922 that diverge from, or near, the megathrust at approximately 30 km depth. This depth is greater  
923 than the 20 km depth of the plate interface beneath splay faults in the PWS region (Brocher et  
924 al., 1994; Liberty et al., 2013; Haeussler et al., 2015), however, this is likely due to simple Pacific  
925 plate subduction below the Kodiak region compared to the additional Yakutat terrane  
926 subduction near PWS (Moore et al., 1991; Ye et al., 1997). Focused uplift along the KSfz near  
927 the Kodiak Islands shoreline exceeds that of the ABfz in the along-dip direction of the  
928 megathrust, and is limited in the along-strike direction by the region of underthrusting to the  
929 southwest and subduction of the 58° fracture zone to the northeast. Wells et al. (2003) inferred  
930 that crustal duplexing might be the source of the unique gravity signal across the Kodiak  
931 Islands. Previous studies near PWS find that splay faulting is assisted by crustal duplexing above  
932 the megathrust (i.e., Liberty et al., 2013 and 2019; Haeussler et al., 2015). Megathrust  
933 duplexing is one hypothesis supporting the observed Kodiak Islands gravity character and uplift  
934 patterns of the KSfz. We do not have complementary constraints on megathrust geometry at  
935 depths greater than 10 km across the central Kodiak Islands, but the Slab2 model (Hayes et al.,  
936 2018) would place the region of duplexing near 25 km depth to the plate interface.

937

#### 938 **CONCLUSIONS**

939 We identify and characterize upper plate splay fault uplift patterns that may be driven by plate  
940 interface conditions. The active faults that we identify have persisted across the Kodiak Islands  
941 offshore region during many Holocene megathrust earthquakes. Subduction of fracture zones,  
942 seamounts, and sediments may drive megathrust segmentation and delimit where active splay  
943 faults are found along the Gulf of Alaska margin.

944

945 A near-shore tsunami risk is present for coastal populations on mainland Kodiak Island. Our  
946 tsunami modelling offers an updated view on how tsunamigenic faults uplift in response to  
947 megathrust slip offshore of the Kodiak Islands. We find that a short region of the Kodiak Shelf  
948 fault zone is consistent with the tsunami source during the GAE because a majority of

949 propagated wave fronts converge to one location where we image tall fault scarps (>20 m). We  
950 term this tsunamigenic fault the Ugak fault. This fault, and parallel faults of the KSfz should be  
951 included in seismic and tsunami hazard analysis of the region.

952

953 Overall, the spatial variability in the KSfz seafloor scarp height indicates discrete, short (< 30  
954 km) uplift patterns, and thus fault segmentation. More detailed, high-resolution bathymetric  
955 and seismic reflection data would help to further constrain fault characteristics and slip-rates,  
956 especially near proposed segment boundaries.

957

#### 958 **DATA AND RESOURCES**

959 For our tsunami source and fault mapping analysis, we utilize a regional bathymetry dataset to  
960 identify Kodiak shelf seafloor scarps (National Geophysical Data Center, 2009. Southern Alaska  
961 Coastal Relief Model. National Geophysical Data Center, NOAA. doi:10.7289/V58G8HMQ).  
962 Seafloor topographic data are available from NOAA at  
963 <https://www.ngdc.noaa.gov/mgg/bathymetry/hydro.html>. The legacy seismic profiles were  
964 obtained as digital scans of stacked travel time images from MMS permit 75-02  
965 (<https://www.boem.gov/Geological-and-Geophysical-Data-Acquisition-and-Analysis/>; Liberty,  
966 2013). EMAG2: Earth Magnetic Anomaly Grid (Stefan Maus, 2009) was obtained from the  
967 National Geophysical Data Center, NOAA. Model. doi:10.7289/V5MW2F2P. Global marine  
968 gravity model from CryoSat-2 and Jason-1 was obtained from the National Geophysical Data  
969 Center at <https://data.noaa.gov> (Sandwell et al., 2014).

970

#### 971 **ACKNOWLEDGEMENTS**

972 We thank the Associate Editor Craig H. Jones and two anonymous reviewers for their  
973 constructive evaluation of this paper. We also thank R/V Alaska Gyre Captain Greg Snegden for  
974 his help with the 2015 marine seismic data acquisition and acknowledge the careful, thoughtful  
975 reviews of an earlier version of this study by Drake Singleton. The authors acknowledge funding  
976 from this work through U.S. Geological Survey award number G15AP00042. Any use of trade,  
977 firm, or product names is for descriptive purposes only and does not imply endorsement by the  
978 U.S. Government.

979

980 REFERENCES

- 981 Barcheck, G., G. Abers, A. N. Adams, A. Becel, J. Collins, J. B. Gaherty, P. J. Haeussler, Z. Li, G.  
982 Moore, E. Onyango, E. Roland, et al., 2020, The Alaska Amphibious Community Seismic  
983 Experiment, *Seismol. Res. Lett.* doi: 10.1785/0220200189.
- 984 Bassett, D., and Watts, A. B., 2015, Gravity anomalies, crustal structure, and seismicity at  
985 subduction zones: 1. Seafloor roughness and subducting relief, *Geochem. Geophys.*  
986 *Geosyst.*, 16, 1508–1540, doi:10.1002/2014GC005684.
- 987 Bécel, A., Shillington, D. J., Delescluse, M., Nedimović, M. R., Abers, G. A., Saffer, D. M., ...  
988 Kuehn, H., 2017, Tsunamigenic structures in a creeping section of the Alaska subduction  
989 zone. *Nature Geoscience*, 10(8), 609–613. <https://doi.org/10.1038/NGEO2990>
- 990 Blakely, R. J. (1996), Potential theory in gravity and magnetic applications. Cambridge university  
991 press. 464 p.
- 992 Briggs, R.W., S. E. Engelhart, A. R. Nelson, T. Dura, A.C. Kemp, P. J. Haeussler, D. R. Corbett, S. J.  
993 Angster, and L.-A. Bradley, 2014, Uplift and subsidence reveal a nonpersistent megathrust  
994 rupture boundary (Sitkinak Island, Alaska), *Geophys. Res. Lett.* 41, 2289–2296.
- 995 Brocher, T. M., G. S. Fuis, M. A. Fisher, G. Plafker, M. J. Moses, J. J. Taber, and N. I. Christensen,  
996 1994, Mapping the megathrust beneath the northern Gulf of Alaska using wide-angle  
997 seismic data, *J. Geophys. Res.* 99, 11,663–11,686.
- 998 Bradley, D., Kusky, T., Haeussler, P., Goldfarb, R., Miller, M., Dumoulin, J., Nelson, S.W., Karl, S.  
999 , 2003, Geologic signature of an early Tertiary ridge subduction in Alaska. In: Sisson, V. B.,  
1000 Roeske, S. M., Pavlis, T. L. (Eds.), *Geology of the Transpressional Oregon Developed During*  
1001 *– Trench Interaction Along the North Pacific Margin, 19-49, Geol. Soc. Am. Spec. Pap. 371.*
- 1002 Bruns, T.R., 1983, Model for the origin of the Yakutat block, an accreting terrane in the northern  
1003 Gulf of Alaska, *Geology*, 11 (12), 718–721.
- 1004 Carlson, P.R. and Molnia, B.F., 1975, Preliminary isopach map of Holocene sediments, northern  
1005 Gulf of Alaska. Scale 1:500,000: *U.S. Geol. Surv., Open-File Rep.*, 75-507, 1 map sheet.
- 1006 Carver, G., and G. Plafker, 2008, Paleoseismicity and neotectonics of the Aleutian Subduction  
1007 Zone—An overview, in *Active Tectonics and Seismic Potential of Alaska, Geophys. Monogr.*  
1008 *Ser. 179*, edited by J. T. Freymueller et al., pp. 43–63, AGU, Washington, D. C.,  
1009 doi:10.1029/179GM03.
- 1010 Carver, G., Sauber, J., Lettis, W., Witter, R. and Whitney, B., 2008, Active faults on northeastern  
1011 Kodiak island, Alaska. *Geophysical Monograph Series, 179*(December 2015), 167–184.  
1012 <https://doi.org/10.1029/179GM09>
- 1013 Cohen, S. C., and J. T. Freymueller, 2004, Crustal deformation in the south central Alaska  
1014 subduction zone, *Adv. Geophys.*, 47, 1–63.

- 1015 Cramer, F., 2018, Scientific colour-maps. Zenodo. <http://doi.org/10.5281/zenodo.1243862>  
1016 (accessed November 2021).
- 1017 Doser, D., Brown, W. A., and Velasquez, M., 2002, Seismicity of the Kodiak Island region (1964-  
1018 2001) and its relation to the 1964 Great Alaska Earthquake, *Bull. Seismol. Soc. Am.*, 92,  
1019 3269-3292.
- 1020 Doser, D., 2005, Historical Seismicity (1918-1964) of the Kodiak Island Region, *Bull. Seismol. Soc.*  
1021 *Am.* 95, no. 3, 878-895, doi: 10.1785/0120040175.
- 1022 Eberhart-Phillips, D., D. H. Christensen, T. M. Brocher, R. Hansen, N. A. Ruppert, P. J. Haeussler,  
1023 and G. A. Abers, 2006, Imaging the transition from Aleutian subduction to Yakutat collision  
1024 in central Alaska, with local earthquakes and active source data, *J. Geophys. Res.* 111,  
1025 B11303, doi:10.1029/2005JB004240.
- 1026 Finn, S. P., L.M. Liberty, P.J. Haeussler and T.L. Pratt, 2015, Landslides and megathrust splay  
1027 faults captured by the late Holocene sediment record of eastern Prince William Sound,  
1028 Alaska. *Bull. Seismol. Soc. Am.* 105, no. 5, 2343–2353. <https://doi.org/10.1785/0120140273>
- 1029 Fisher, M. A., 1980, Petroleum geology of Kodiak shelf, Alaska. *AAPG Bull.*, 64, no. 8, 1140-1157.
- 1030 Fisher, M. A., and von Huene, R., 1980, Structure of the upper Cenozoic strata beneath Kodiak  
1031 shelf, Alaska, *AAPG Bull.* 64, 1014–1033.
- 1032 Fruehn, J., von Huene, R., and Fisher, M., 1999, Accretion in the wake of terrane collision: The  
1033 Neogene accretionary wedge off Kenai Peninsula, Alaska, *Tectonics*, 18, 263-277.
- 1034 Fuller, C. W., Willett, S. D. and Brandon, M.T., 2006. Formation of forearc basins and their  
1035 influence on subduction zone earthquakes. *Geology*, 34, no. 2, 65-68.
- 1036 Gulick, S. P. S., Jaeger, J. M., Mix, A. C., Asahi, H., Bahlburg, H., Belanger, C. L., ... Swartz, J. M.  
1037 2015, Mid-Pleistocene climate transition drives net mass loss from rapidly uplifting St. Elias  
1038 Mountains, Alaska. *Proceedings of the National Academy of Sciences* 112, 15042–15047.  
1039 <https://doi.org/10.1073/pnas.1512549112>.
- 1040 Gutscher, M. A., Kukowski, N., Malavieille, J., and Lallemand, S., 1998). Episodic imbricate  
1041 thrusting and underthrusting: Analog experiments and mechanical analysis applied to the  
1042 Alaskan accretionary wedge. *J. Geophys. Res.* 103, no. B5, 10161-10176.
- 1043 Haeussler, P. J., Armstrong, P. A., Liberty, L. M., Ferguson, K. M., Finn, S. P., Arkle, J. C., and  
1044 Pratt, T. L., 2015, Focused exhumation along megathrust splay faults in Prince William  
1045 Sound, Alaska, *Quat. Sci. Rev.* 113, 8-22.
- 1046 Hayes, G., 2018, Slab2 - A Comprehensive Subduction Zone Geometry Model: U.S. Geological  
1047 Survey data release, <https://doi.org/10.5066/F7PV6JNV>.

- 1048 Hutchinson, I. and Crowell, A., 2007, Recurrence and extent of great earthquakes in southern  
1049 alaska during the late Holocene from an analysis of the radiocarbon record of land-level  
1050 change and village abandonment, *Radiocarbon*, 49, 3, 1323-1385.
- 1051 Johnson, J. M., Satake, K., Holdahl, S. R., and Sauber, J., 1996, The 1964 Prince William Sound  
1052 earthquake: joint inversion of tsunami and geodetic data, *J. Geophys. Res.*, 101(B1), 523-  
1053 532.
- 1054 Kachadoorian, R. and Plafker, G., 1967, Effects of the earthquake of March 27 1964 on the  
1055 communities of Kodiak and nearby islands: U.S. Geological Survey Professional Paper 542-F,  
1056 p. F1-F41.
- 1057 Kaufman, D. S., and W. F. Manley, 2004, Pleistocene maximum and Late Wisconsin glacier  
1058 extents across Alaska, U.S.A., in *Quaternary Glaciations—Extent and Chronology, Part II:  
1059 North America. Developments in Quaternary Science*, vol. 2, edited by J. Ehlers, and P. L.  
1060 Gibbard, pp. 9–27, Elsevier, Amsterdam.
- 1061 Kaufman, D.S., Young, N.E., Briner, J.P. and Manley, W.F., 2011, Alaska palaeo-glacier atlas  
1062 (version 2), *Dev. Quat. Sci.*, 15, 427-445. [https://doi.org/10.1016/B978-0-444-53447-  
1063 7.00033-7](https://doi.org/10.1016/B978-0-444-53447-7.00033-7)
- 1064 Kelsey, H.M., Witter, R. C., Engelhart, S. E., Briggs, R., Nelson, A., Haeussler, P. J., and Corbett, D.  
1065 R., 2015, Beach ridges as paleoseismic indicators of abrupt coast subsidence during  
1066 subduction zone earthquakes, and implications for Alaska-Aleutian subduction zone  
1067 paleoseismology, southeast coast of the Kenai Peninsula, Alaska, *Quat. Science Rev.*, 113,  
1068 147-158.
- 1069 Kim, Y., Abers, G. A., Li, J., Christensen, D., Calkins, J., and Rondenay, S., 2014, Alaska  
1070 Megathrust 2: Imaging the megathrust zone and Yakutat/Pacific plate interface in the  
1071 Alaska subduction zone, *J. Geophys. Res.* 119, 1924–1941, doi:10.1002/2013JB010581
- 1072 Ichinose, G., Somerville, P., Thio, H. K., Graves, R., and O’Connell, D., 2007, Rupture process of  
1073 the 1964 Prince William Sound, Alaska, earthquake from the combined inversion of  
1074 seismic, tsunami, and geodetic data, *J. Geophys. Res.*, 112, doi:10.1029/2006JB004728.
- 1075 Lamb, H. (1932) *Hydrodynamics*. 6th Edition, Cambridge University Press, Cambridge, 1-8
- 1076 Lebrun, J. F., Karner, G. D., and Collot, J. Y., 1998, Fracture zone subduction and reactivation  
1077 across the Puysegur ridge/trench system, southern New Zealand, *J. Geophys. Res.*, 103,  
1078 7293-7313.
- 1079 Li, J., Abers, G. A., Kim, Y. H., and Christensen, D., 2013, Alaska megathrust 1: Seismicity 43  
1080 years after the great 1964 Alaska megathrust earthquake, *J. Geophys. Res.: Solid Earth*,  
1081 118, 4861–4871, doi:10.1002/jgrb.50358.

- 1082 Li, J., Shillington, D. J., Saffer, D. M., Bécel, A., Nedimović, M. R., Kuehn, H., ... Abers, G. A., 2018,  
1083 Connections between subducted sediment, pore-fluid pressure, and earthquake behavior  
1084 along the Alaska megathrust. *Geology*, 46(4), 299–302. <https://doi.org/10.1130/G39557.1>
- 1085 Li, S., Freymueller, J., and McCaffrey, R., 2016, Slow slip events and time-dependent variations  
1086 in locking beneath Lower Cook Inlet of the Alaska-Aleutian subduction zone, *J. Geophys.*  
1087 *Res. Solid Earth*, 121, doi:10.1002/2015JB012491.
- 1088 Liberty, L. M., 2013, Retrieval, Processing, Interpretation and Cataloging of Legacy Seismic  
1089 Reflection Data, Gulf of Alaska, US Geological Survey Final Technical Report G12AP20078,  
1090 17 p., [https://earthquake.usgs.gov/cfusion/external\\_grants/reports/G12AP20078.pdf](https://earthquake.usgs.gov/cfusion/external_grants/reports/G12AP20078.pdf)
- 1091 Liberty, L.M., 2015, Near Surface Expression of Megathrust Splay Faults, Western Gulf of Alaska,  
1092 US Geological Survey Final Technical Report #G13AP00021, 17 p,  
1093 [https://earthquake.usgs.gov/cfusion/external\\_grants/reports/G13AP00021.pdf](https://earthquake.usgs.gov/cfusion/external_grants/reports/G13AP00021.pdf)
- 1094 Liberty, L.M. and Ramos, M. D., 2016, Co-seismic rupture patterns over multiple earthquake  
1095 cycles near Kodiak Island: a collaborative project with USGS personnel, US Geological  
1096 Survey Final Technical Report #G13AP00021, 17 p,  
1097 [https://earthquake.usgs.gov/cfusion/external\\_grants/reports/G15AP00042.pdf](https://earthquake.usgs.gov/cfusion/external_grants/reports/G15AP00042.pdf)
- 1098 Liberty, L. M., Finn, S. P., Haeussler, P. J., Pratt, T. L., and Peterson, A., 2013, Megathrust splay  
1099 faults at the focus of the Prince William Sound asperity, Alaska, *J. Geophys. Res.* 118, no.  
1100 10, 5428–5441. <http://doi.org/10.1002/jgrb.50372>.
- 1101 Liberty, L. M., Brothers, D. S., and Haeussler, P.J., 2019, Tsunamigenic splay faults imply a long-  
1102 term asperity in southern Prince William Sound, Alaska. *Geophys. Res. Lett.* 46, 3764–  
1103 3772. <https://doi.org/10.1029/2018GL081528>
- 1104 Maus, S., 2009, EMAG2: Earth Magnetic Anomaly Grid (2-arc-minute resolution). National  
1105 Geophysical Data Center, NOAA. Model. doi:10.7289/V5MW2F2P [May 2016].
- 1106 Moore, J. C., Bryne, T., Plumely, P. W., Reid, M., Gibbons, H., and Coe, R. S., 1983, Paleogene  
1107 evolution of the Kodiak Islands, Alaska: Consequences of ridge-trench interaction in a more  
1108 southerly latitude, *Tectonics*, 2, 265-293.
- 1109 Moore, J. C., et al., 1991, EDGE deep seismic reflection transect of the eastern Aleutian arc-  
1110 trench layered lower crust reveals underplating and continental growth, *Geology*, 19, 420-  
1111 424.
- 1112 Mankhemthong, N., Doser, D. I., & Pavlis, T. L., 2013, Interpretation of gravity and magnetic  
1113 data and development of two-dimensional cross-sectional models for the border ranges  
1114 fault system, south-central alaska. *Geosphere*, 9(2), 242–259.  
1115 <https://doi.org/10.1130/GES00833.1>

- 1116 Menard, H. W. and Atwater, T., 1969, Origin of fracture zone topography. *Nature*, 222(5198),  
1117 1037-1040.
- 1118 Meyer, B, Saltus, R., and Chulliat, A., 2017, EMAG2v3: Earth Magnetic Anomaly Grid (2-arc-  
1119 minute resolution). Version 3. NOAA National Centers for Environmental Information.  
1120 <https://doi.org/10.7289/V5H70CVX>. Accessed July 2, 2021.
- 1121 Naugler, F. P. and Wageman, J. M., 1973, Gulf of Alaska: Magnetic Anomalies, Fracture Zones,  
1122 and Plate Interaction, *GSSA Bull.*, 84, 1575-1584.
- 1123 Nishenko, S. P. and Jacob, K. H., 1990, Seismic potential of the Queen Charlotte-Alaska-Aleutian  
1124 seismic zone. *J. Geophys. Res.* **95**, no. B3, 2511–2532,  
1125 <https://doi.org/10.1029/JB095iB03p02511>
- 1126 NOAA National Centers for Environmental Information. 2004: Multibeam Bathymetry Database  
1127 (MBBDB). NOAA National Centers for Environmental Information.  
1128 <https://doi.org/doi:10.7289/V56T0JNC>. Accessed [date].
- 1129 Plafker, G., 1969, Tectonics of the March 27, 1964 Alaska earthquake, *U.S. Geol. Surv. Prof.*  
1130 *Pap.*, 543-I, 74 pp.
- 1131 Plafker, George, and Berg, H.C., eds., 1994, *The Geology of Alaska*: Geological Society of  
1132 America, 1068 p.
- 1133 Porto, N. M. and Fitzenz, D. D., 2016, An alternative segmentation model for the Alaskan  
1134 Aleutian megathrust. *Bull. Seismol. Soc. Am.* **106**, no. 3, 1125–1132.  
1135 <https://doi.org/10.1785/0120150235>
- 1136 Reece, R.S., Gulick, S.P.S., Horton, B.K., Christeson, G.L., and Worthington, L.L., 2011, Tectonic  
1137 and climatic influence on the evolution of the Surveyor fan and channel system, Gulf of  
1138 Alaska, *Geosphere*, **7**, 4, 830–844, doi: 10.1130/GES00654.1.
- 1139 Robinson, D. P. and Watts, A. B., 2006, Earthquake rupture stalled by a subducting fracture  
1140 zone, *Science*, **312**, 1203-1205.
- 1141 Ryan, H.F., von Huene, R., Wells, R.E., Scholl, D.W., Kirby, S., and Draut, A.E., 2011, History of  
1142 earthquakes and tsunamis along the eastern Aleutian-Alaska megathrust, with implications  
1143 for tsunami hazards in the California continental borderland: U.S. Geological Survey  
1144 Professional Paper 1795-A, 31 p.
- 1145 Sandwell, D. T., 1984, Thermomechanical evolution of oceanic fracture zones, *J. Geophys. Res.*,  
1146 **89** (B13), 11401-11113
- 1147 Sandwell, D. T., Müller, R. D., Smith, W. H. F., Garcia, E., Francis, R., 2014, New global marine  
1148 gravity model from CryoSat-2 and Jason-1 reveals buried tectonic structure, *Science*, **346**  
1149 (6205), 65-67, doi: 10.1126/science.1258213.

- 1150 Saltus, R. W., Hudson, T. L., and Wilson, F. H. 2007, The geophysical character of southern  
1151 Alaska—Implications for crustal evolution, in Tectonic Growth of a Collisional Continental  
1152 Margin: Crustal Evolution of Southern Alaska, USA, K. D. Ridgway, J. M. Trop, J. M. G. Glen,  
1153 and J. M. O'Neill (Editors), Geol. Soc. Am. Spec. Pap. 431, Boulder, Colorado, 1–20.
- 1154 Sauber, J., Carver, G., Cohen, S., and King, R., 2006, Crustal deformation and the seismic cycle  
1155 across the Kodiak Islands, Alaska, *J. Geophys. Res.*, **111**, B02403,  
1156 doi:10.1029/2005JB003626.
- 1157 Shennan, I., Barlow, N., Carver, G., Davies, F., Garrett, E., and Hocking, E., 2014, Great  
1158 tsunamigenic earthquakes during the past 1000 yr on the Alaska megathrust, *Geology*, **42**,  
1159 687-690.
- 1160 Shennan, I., Brader, M. D., Barlow, N. L. M., Davies, F. P., Longley, C., & Tunstall, N., 2018, Late  
1161 Holocene paleoseismology of Shuyak Island, Alaska, *Quat. Sci. Rev.* **201**, 380–395.  
1162 <https://doi.org/10.1016/j.quascirev.2018.10.028>
- 1163 Shillington, D.J.; Bécel, A., Nedimović, M.R., Kuehn, H., Webb, S.C. Abers, G.A., Keranen, K.M.;  
1164 Li, J.; Delecluse, M.; Mattei-Salicrup, G.A., 2015, Link between plate fabric, hydration and  
1165 subduction zone seismicity in Alaska, *Nature Geosci.*, **8**, 961-964, doi:10.1038/ngeo02586
- 1166 Smith, W. H. F. and Sandwell, D. T., 1997, Global seafloor topography from satellite altimetry  
1167 and ship depth soundings, *Science*, **277**, 1957-1962.
- 1168 Song, T. A. and Simons, M., 2003, Large trench-parallel gravity variations predict seismogenic  
1169 behavior in subduction zones, *Science*, **301**, 630-632.
- 1170 Suleimani, E., and Freymueller, J. T., 2020, Near-field modeling of the 1964 Alaska tsunami: The  
1171 role of splay faults and horizontal displacements, *J. Geophys. Res. Solid Earth* **125**, 1–23,  
1172 doi: 10.1029/ 2020JB019620.
- 1173 Suito, H., and Freymueller, J. T., 2009, A viscoelastic and afterslip postseismic deformation  
1174 model for the 1964 Alaska earthquake, *J. Geophys. Res.* **114**, doi:10.1029/ 2008JB005954.
- 1175 von Huene, R., Hampton, M., Fisher, M., Varchol, D., and Cochrane, G., 1980, Map showing  
1176 near-surface geologic structures of Kodiak Shelf, Alaska, *U.S. Geol. Surv. Miscellaneous Field  
1177 Studies Map MF-1200*, 1 sheet, 1:500,000 scale.
- 1178 von Huene, R., Fisher, M. A., and Bruns, T. R., 1987, Geology and evolution of the Kodiak  
1179 margin, Gulf of Alaska, in Geology and Resource Potential of the Continental Margin of  
1180 Western North America and Adjacent Ocean Basins-Beaufort Sea to Baja California, Scholl,  
1181 D. W., Grantz, A., and Vedder, J. G., (eds.): Houston, Texas, Circum-Pacific Council for  
1182 Energy and Mineral Resources, p. 191-212.



- 1183 von Huene, R., Klaeschen, D., and Fruehn, J., 1999, Relation between the Subducting Plate and  
1184 Seismicity Associated with the Great 1964 Alaska Earthquake, *Pure and App. Geophys.*, 154,  
1185 575-591.
- 1186 von Huene, R., Miller, J. J., and Weinrebe, W., 2012, Subducting plate geology in three great  
1187 earthquake ruptures of the western Alaska margin, Kodiak to Unimak, *Geosphere*, 8(3),  
1188 628–644.
- 1189 Wang, K., and Hu, Y., 2006, Accretionary prisms in subduction earthquake cycles: The theory of  
1190 dynamic Coulomb wedge, *J. Geophys. Res.*, 111, B06410, doi:10.1029/2005JB004094.
- 1191 Wang, K. and Bilek, S., 2011, Do subducting seamounts generate or stop large earthquakes?  
1192 *Geology*, 39, 819-822.
- 1193 Wells, D. L., and Coppersmith, K. J., 1994, New Empirical Relationships among Magnitude,  
1194 Rupture Length, Rupture Width, Rupture Area, and Surface Displacement. *Bull. Seismol.*  
1195 *Soc. Am.* 84, no. 4, 974–1002.
- 1196 Wells, R. E., Blakely, R. J., Sugiyama, Y., Scholl, D. W., and Dinterman, P. A., 2003, Basin-  
1197 centered asperities in great subduction zone earthquakes: A link between slip, subsidence,  
1198 and subduction erosion?, *J. Geophys. Res.*, 108(B10), 2507, doi:10.1029/2002JB002072.
- 1199 Ye, S., Flueh, E. R., Klaeschen, D., and von Huene, R., 1997, Crustal structure along the EDGE  
1200 transect beneath the Kodiak shelf off Alaska derived from OBH seismic refraction data,  
1201 *Geophys. J. Int.*, 130, 283-302.
- 1202 Zimmermann, M., Prescott, M.M. and Haeussler, P.J., 2019, Bathymetry and geomorphology of  
1203 Shelikof Strait and the Western Gulf of Alaska. *Geosciences*, 9(10), p.409.
- 1204 Zweck, C., Freymueller, J. T., and Cohen, S. C., 2002, Three-dimensional elastic dislocation  
1205 modeling of the postseismic response to the 1964 Alaska earthquake, *J. Geophys. Res.*, 107,  
1206 10.1029/2001.  
1207

1208 **Table 1.** Tsunami travel times. Travel time difference in the third column is taken to be the  
 1209 relative difference in time between the source convergence point (152.715 W, 57.061 N) and the  
 1210 closest distance to each modeled wave front. Modified from Plafker (1969).

Inundation Site	Travel Time (minutes)	Travel Time Difference (minutes)	First Motion (reported)
Kaguyak	38	6	NA
Old Harbor	48	24	Up
Cape Chiniak	38	0	Up
Kalsin Bay	70	13	NA
Naval Station	63	5	Up
Kodiak City	45	5	Down
Saltery Cove	30	0	NA

1211